Results of the SCK CEN Exercise for Disarmament Verification Technologies

IPNDV Technology Track

November 2021

Abstract

The performance of measurement technologies are important in the framework of developing a verification strategy in a nuclear disarmament scenario. Therefore, the International Partnership for Nuclear Disarmament Verification (IPNDV) has identified testing technologies and procedures as an important step. Belgium proposed and organized at end of 2019 an international exercise at the site of the Belgian Nuclear Research Centre (SCK CEN) in Mol, Belgium. The aim of the exercise was focused on testing and comparing measurement techniques to be potentially used for the verification of nuclear material in the framework of the dismantlement of nuclear weapons. SCK CEN made available well characterized nuclear material in form of Mixed Oxide fuel. The relative content of Pu was up to 14%$_{wt}$ and the isotopic abundance of ^{239}Pu was up to 93%$_{wt}$. The amount of nuclear material being assayed could be chosen by the participants as well the type of an optional shielding material.

Ten measurement teams participated in the exercise deploying different gamma-ray and neutron measurement devices.

This report describes the content of the measurement campaign and the results that were obtained as well their significance for nuclear disarmament verification.

Contents

1 Introduction

The International Partnership for Nuclear Disarmament Verification (IPNDV) focused its work during Phase II, which began in December 2017 and ended in December 2019, on developing effective and practical verification options to support future nuclear disarmament.

The overarching objectives for IPNDV during Phase II were developing effective verification options, including measurement techniques, and demonstrating the work of IPNDV through technology demonstrations.

Regarding these objectives, Belgium proposed, organized, and hosted an international technology exercise at the site of the Belgian Nuclear Research Center (SCK CEN) in Mol, Belgium. This exercise was conducted to test and compare different measurement techniques, and respectively for each technique, evaluate the potential to verify nuclear material within the framework of future nuclear disarmament. The exercise took place in September 2019 with about 30 participants from several countries using different measurement techniques.

Measuring the presence and/or absence of nuclear material with nuclear weapon-related characteristics is likely to form part of future nuclear disarmament efforts that encompass nuclear warheads as treaty accountable items. Together with technologies for chain of custody and, possibly, measurements related to high explosives, they form the potentially available technology tools for verification of nuclear disarmament.

The Belgian exercise, focusing on the measurement technology aspect, also complemented a second nuclear disarmament verification exercise that took place in fall 2019, called “NuDiVe,” because the latter exercise focused on the procedures related to **nu**clear **di**sarmament **ve**rification.

The report begins by detailing the measurement campaign in general and its objectives and possible types of measurements as well as the characteristics and significance of the chosen materials. The results obtained with different technologies are reported in subsequent sections: Gamma-ray measurements detailing high- and medium-resolution detectors are followed by reporting on neutron measurements detailing neutron counters and neutron spectroscopic detectors. Imaging devices are then addressed. Within these sections, each team provided the description of their measurement campaign and their obtained results. Implications for nuclear disarmament verification follows before the conclusions and outlook.

2 Description of the Measurement Campaign

2.1 Objectives and Types of Measurements

The main goal of the measurement campaign was to investigate the performance of different non-destructive passive measurement technologies with respect to their capabilities to verify the presence or absence of nuclear material originating from a nuclear weapon, and distinguish weapon-grade from civil-grade nuclear material.

The material to be assayed was unirradiated mixed oxide (MOX) fuel. The plutonium (Pu) is mixed with uranium (U), chemically in the form of oxide. The total plutonium content is up to 14%$_{wt}$ with a relative ^{239}Pu amount up to 96%$_{wt}$. The MOX fuel pins were arranged in a compact hexagonal configuration as shown in Figure 2-1 to maximize the average density of the item to be assayed.

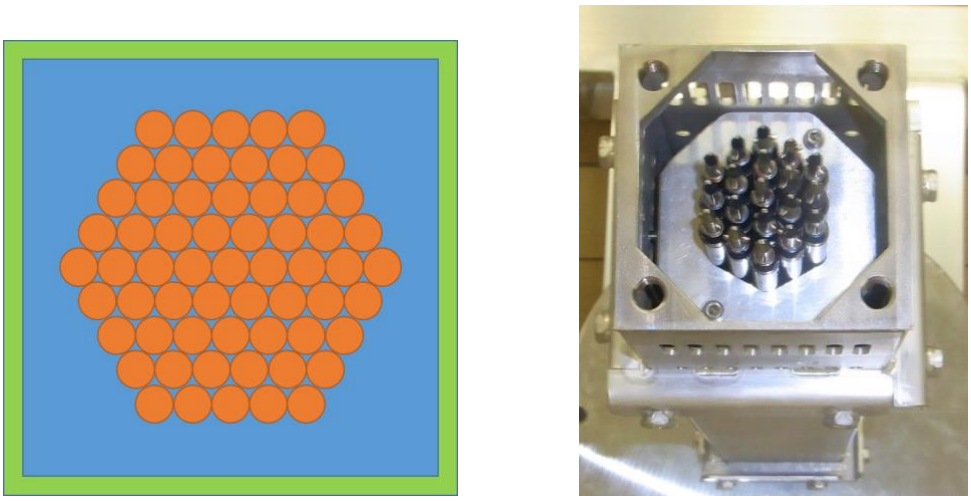

Figure 2-1. (left) Sketch of horizontal cross-section configuration of a container with 61 fuel pins; (right) top view of a 19-pin configuration (Source: SCK CEN. Used by permission)

The composition and geometry of the MOX fuel as well as the design information of the measurement setup is well known and was communicated in advance to the measurement teams. Hence, the data acquired in the exercise provide a sound benchmark to validate developed models for the deployed technologies.

During the measurement campaign it was possible to study the influence on the performance due to the amount of nuclear material, the type of nuclear material, and the type of shielding material. For example, by performing measurements on samples with various amounts of plutonium mass and a fixed isotopic composition, one could study the sensitivity of the methods to the amount of nuclear material. In addition, by measuring samples with different plutonium isotopic compositions, one could assess whether a certain technology was capable of distinguishing between reactor-grade and weapon-grade plutonium. Finally, the performances of the technologies could be assessed in presence of shielding material such as lead (Pb),

cadmium (Cd), and polyethylene (PE). This could represent common shielding of the fissile material due to, for example, safety regulations but could also imply a possibility to divert nuclear material during the dismantling process.

2.2 Characteristics and Significance of the Chosen Materials

A total of five assemblies with given composition were available for the experiments. Emission rates for most intense gamma-rays and neutron emission rates for the considered assemblies are shown in Table 2-1 and Table 2-2. The hexagonal bundle was hosted in a 3 mm thick square container of stainless steel to reduce the gamma-ray dose rate and facilitate the manipulation. The dimensions of the horizontal cross-section of the container were 10 cm × 10 cm. The following individual shielding could be installed on the container: lead 5 mm and 10 mm thick; cadmium 1.1 mm thick; polyethylene 50 mm thick; and/or a combined shielding of polyethylene (50 mm thick on the inside) and lead (10 mm thick on the outside).

The assemblies *62–1, 62–19, 62–61* were fuel pins with a plutonium content of 12.6%$_{wt}$ and with a ^{239}Pu amount of 61%$_{wt}$. The number of rods were 1, 19, or 61; these numbers allowed to keep a hexagonal arrangement and to have a ^{239}Pu mass range from 0.1 to 2.6 kg. The uranium enrichment was 0.4%. These assemblies could be used for measurements dedicated to the study of the mass determination or sensitivity.

The assemblies *62–19, 79–19* and *96–19* had a ^{239}Pu relative content in the PuO_2 of 61%$_{wt}$, 79%$_{wt}$, and up to 96%$_{wt}$ respectively. The *96–19* was an axially heterogeneous assembly ^{239}Pu relative content of 79% at the top and bottom and 96%$_{wt}$ at the mid of the assembly. Among these assemblies, the plutonium content ranged between 4%$_{wt}$ and 12%$_{wt}$ and the uranium enrichment was between 0.4% and 2.0%. These assemblies could be used for measurements dedicated to determine the isotopic composition.

Assembly ID	^{240}Pu 160 keV	^{235}U 186 keV	^{239}Pu 413 keV	^{239}Pu 646 keV	^{240}Pu 642 keV	^{241}Am 662 keV	^{238}U 1001 keV
79–19	1,605	161	7,482	75	50	3,567	386
96–19	660	319	5,598	56	20	1,345	373
62–1	539	7	1,436	14	17	2,364	30
62–19	10,243	134	27,292	273	318	44,907	576
62–61	32,887	430	87,621	876	1,022	144,174	1,850

Table 2-1. Emission rates for most intense gamma-rays for the considered assemblies (values expressed in 10^3 photons/s)

Assembly ID	Spontaneous fission			(α,n) reaction		
	Pu	U	Am	Pu	U	Am
79–19	51	0.1	<0.1	17	0.5	21
96–19	21	0.1	<0.1	10	0.5	8
62–1	23	<0.1	<0.1	13	<0.1	14
62–19	439	0.1	<0.1	241	0.7	262
62–61	1,410	0.3	<0.1	774	2.1	841

Table 2-2. Neutron emission rates for the considered assemblies (values expressed in 10^3 neutron/s)

The plutonium used in the measurement campaign differs from the envisaged material in a nuclear explosive device to be inspected during a disarmament verification process for the aspects outlined in Table 2-3.

	Exercise	Warhead
Material	Civil/weapon grade plutonium mixed with depleted/natural/low enriched uranium	Weapon grade plutonium metal (+depleted uranium as reflector)
Chemical form	Oxide	Metal
Geometry	Hexagonal bundle of pins	(quasi)spherical
Impurities	^{241}Am from ^{241}Pu decay (30÷85 mg/g_{Pu})	^{241}Am from ^{241}Pu decay (0 ÷ 30 mg/g_{Pu})

Table 2-3. Characteristics of the materials measured in the exercise and in a nuclear warhead

When considering a detection system based on gamma-ray spectroscopy, the differences outlined in Table 2-3 have an impact on the detector response. Although the gamma-ray emission of plutonium does not depend on the chemical form, its density, composition, and geometry affect the degree of attenuation to which the gamma radiation undergoes. The data in Table 2-1 indicate that the gamma-lines from both uranium and ^{241}Am should be visible in the spectra, which this would complicate the spectral analysis when compared to the one associated with a real warhead.

When considering a detection system based on neutron coincidence counting, although the neutron emission due to spontaneous fission does not depend on the chemical form, there is a significant (α,n) component associated due to the fact that the material is in oxide form; the data in Table 2-2 reveal that this contribution is estimated to be comparable to the contribution from spontaneous fission. The total neutron emission is therefore depending on the chemical form. Due to the non-negligible multiplication, the (α,n) component is expected to have an impact also on the number of coincident neutrons being detected. We expect therefore that the time uncorrelated component associated to the (α,n) reaction makes the measurements and interpretation of the data more difficult when compared to a plutonium in metal form.

Given these considerations, the verification of well-characterized MOX fuel may even be more challenging than the one of a nuclear explosive device. In addition to testing the technologies in a complex scenario, the proposed exercise provides a sound benchmark to validate developed models for verification devices based on the deployed technologies.

2.3 Participating Teams

About 30 people representing the delegations of Australia, Belgium, Canada, the European Union, Finland, Hungary, Japan, Norway, Switzerland, and the United Kingdom, participated to the experimental campaign. The Nuclear Threat Initiative (NTI) was present as observer at the beginning of the campaign. Germany provided support for calculations and during the Belgian measurements.

Participants deployed different measurement instruments. We can categorize them as follows: Gamma-ray detectors (either low-/medium- or high-resolution), neutron detectors (either total counters or neutron coincidence counters), imaging devices (gamma-rays and neutrons). The next sections of the report describe the results from the different measurement instruments.

3 Gamma Measurements

3.1 High-Resolution Detectors

3.1.1 Belgium (SCK CEN)

The goal of the measurement was to verify special nuclear material (SNM) in bare form or with minimal amount of shielding by deploying a low-energy germanium (LEGe) detector and analyzing the collected gamma-ray spectra. In particular, the performance of the technology was assessed with respect to its ability to determine the plutonium isotopic composition, time since last separation, and ^{235}U/Pu and ^{238}U/Pu ratios.

Detector and Setup

High-resolution gamma-ray measurements between 0 and 300 keV were carried out with a LEGe detector from Canberra,[1] and cooled with liquid nitrogen. The resolution at 59.5 keV is 0.62 keV, at 208 keV is 0.83 keV, which is worse than the one recommended[2] for the data analysis (0.55 keV at 122 keV). The data acquisition is done with the Genie software in combination with an Inspector 2000[3] from Canberra/Mirion.

A lead collimator was used to limit scattered radiation ((a) (b)

Figure 3-1). Measurement times were between 12–30 minutes with a distance between 2.5–25 cm. The distance was chosen to limit the dead time to few percent.

[1] Low Energy Germanium Detector, Mirion Technologies, http://www.gammadata.se/assets/Uploads/LEGe-SS-C49322.pdf.

[2] T. Sampson, "*Plutonium Isotopic Analysis Using PC/FRAM*" LA-UR-03-4403, 2007.

[3] M.J. Koskelo, W.A. Sielaff, D.L. Hall, M.H. Kastner, & V.T. Jordanov, (2001), "*Inspector-2000 A DSP-Based, Portable, Multi-Purpose MCA,*" *Journal of Radioanalytical and Nuclear Chemistry 248* (2), 257–262.

Given that only low-energy gamma-rays are considered, there is a significant self-absorption in the sample and therefore the method assays only the outer part of the sample; in combination with a narrow collimator, this limits the spatial region to which the detector is sensitive. Measurements with lead shielding were not carried out as almost no gamma-rays that could be detected would have reached the detector. However, a 1.1 mm thick Cd shielding was used to limit the count rate due to the 60 keV gamma-ray line of ^{241}Am.

Measured Samples

The measured samples consisted of 19-pin hexagonal bundles, *96–19, 79–19,* and *62–19* measured at the mid-axial position. In addition, the *96–19* was measured at the bottom axial position where the ^{239}Pu relative content is 79%$_{wt}$.

Figure 3-2 shows the spectra obtained with the LEGe detector for the *96–19*, *79–19,* and *62–19* measured at the mid-axial positions.

(a) **(b)**

Figure 3-1. Setup of the measurement with the LEGe detector: (a) a Cd shielding covers the assembly; (b) lead collimator is present in front of the detector. (Source: SCK CEN. Used by permission)

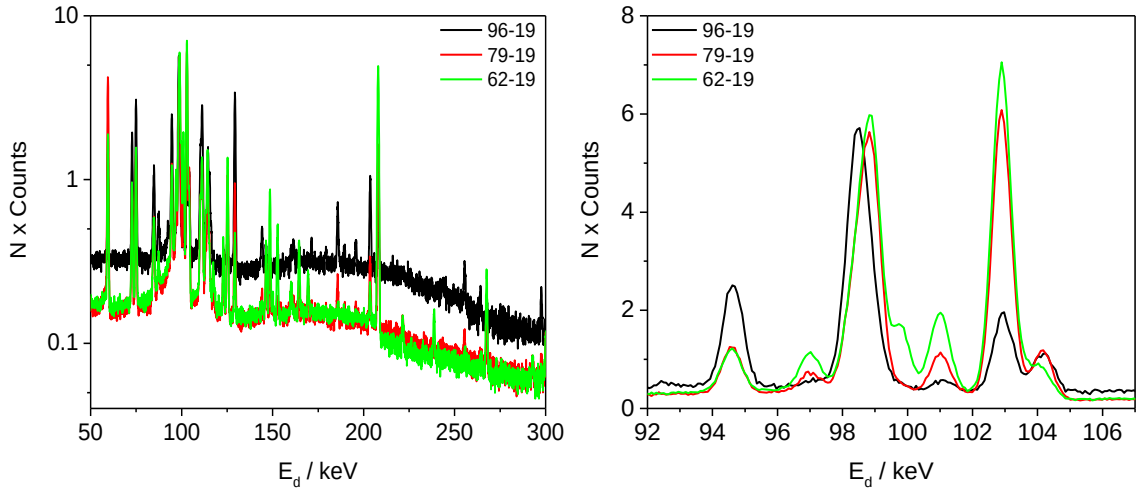

Figure 3-2. Obtained spectra with the LEGe detector for three samples

Analysis and Results

The data analysis was carried out with the FRAM[4] code version 4. The parameter set *UPu60_210SolidX* for Planar detector (0.075 keV/ch, ^{235}U/Pu < 1, 60–210 keV with physical model of the efficiency) was used with its default settings. The analysis is applicable only to spatially homogenously distributed samples containing SNM.

We could determine that the different content of ^{241}Am strongly affects the observed response in Figure 3-2, for example with its peaks at 98.95 keV, 101.07 keV, and 102.96 keV.

The obtained results for all four samples revealed that:

- The relative uncertainty on ^{239}Pu is 0.2÷0.8%, the relative bias is at most 2.5%.
- The relative uncertainty on ^{240}Pu is 2÷6%, the relative bias is at most 13%.
- The relative uncertainty on the separation time is less than 2%, the relative bias is at most 3%.
- The ^{242}Pu was estimated using correlation curves available in FRAM. The estimate of ^{242}Pu for the case *96–19 mid* where ^{239}Pu relative content is the highest, the ^{242}Pu content could not be well determined. However, the ^{242}Pu content is less than 0.1%.
- The ratio U/Pu from analysis of the x-ray region could not be determined in a satisfactory way.

Conclusions

We could conclude that the technology can distinguish civil from military-grade plutonium as well as the time from last separation, despite the increased background conditions (^{241}Am).

The method was tested in conditions with limited shielding (3 mm stainless steel + 1.1 mm Cd) and we did not test from which shielding thickness the method fails. The measurements were done only up to 300 keV; extending the range to 450 keV is a possibility that should be explored

[4] T. Sampson, "*Plutonium Isotopic Analysis Using PC/FRAM*" LA-UR-03-4403, 2007.

because in principle it should be less sensitive to shielding. The measurement time is in the order of 10 minutes, which is acceptable for verification inspections. The fact that the technology works only with limited shielding limits its applicability to the steps in the disarmament scenario where the SNM has been removed from the warhead and structural components.

Given the fact that sensitive information, such as radionuclide vector of plutonium can be revealed an information barrier, similar to what described in the UK-Norway Initiative[5], should be in place for its deployment.

3.1.2 Switzerland (Spiez Laboratory)

Configuration Used, Detector Specification

Two Falcon 5000 units on a laboratory cart were used to simultaneously record spectra of different energy ranges (Figure 3-3). The Falcon 5000 is a portable, electrically cooled gamma spectrometry system with a high-purity germanium detector (HPGe) with a relative efficiency of about 23%z[6] from Mirion (Canberra). The height of the laboratory cart could be adjusted so that the center of the germanium crystal was level with the center of the fuel elements. The distance to the fuel element was originally intended to be such that the detectors would measure only the center ± 10 cm. As the count rates proved to be too high at such a small distance, it was increased and therefore the whole fuel elements were measured.

Figure 3-3. Two Falcon 5000 units on a height-adjustable laboratory trolley. A collimator made of lead, with a thin copper foil on the side facing the detector, was built around the two detectors (and fixed with green tape) (Source: SCK CEN. Used by permission)

[5] "*High Level Requirements for the UKNI Information Barrier*" available at https://ukni.info/document-library/
[6] Compared to 3 × 3" NaI(Tl), point source of Co-60 in 25 cm.

Spectra

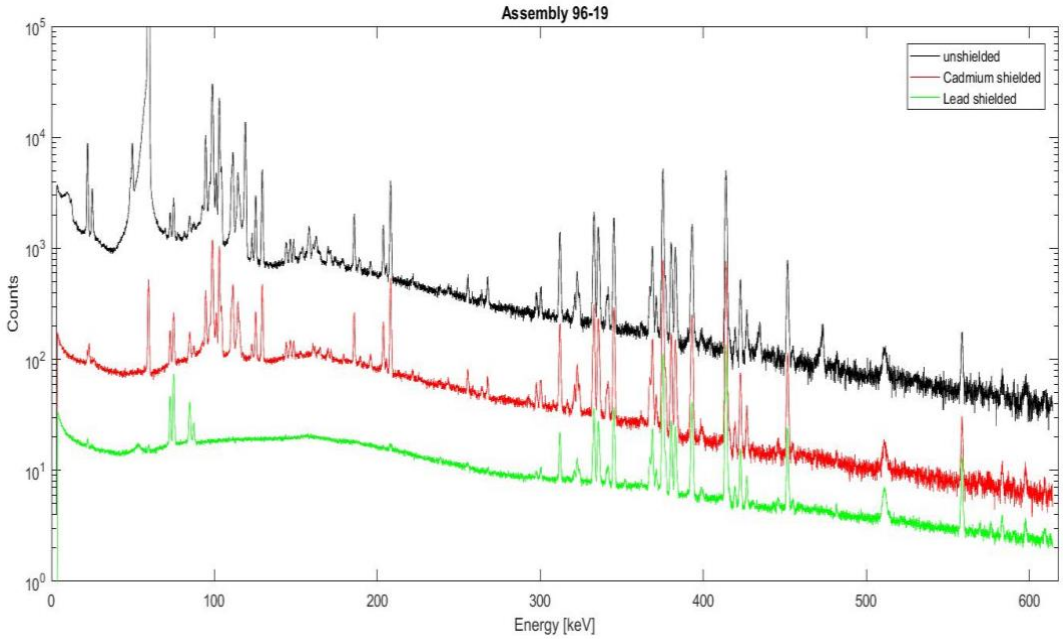

Figure 3-4. Spectra of the 96-19 assembly measured without shielding (black), behind cadmium shielding (red) and behind lead shielding (green). For better visibility, the red and green spectra have been shifted downward.

Figure 3-4 shows the effects of shielding using the example of the spectra of 96-19. With cadmium shielding the 60 keV ^{241}Am peak is considerably attenuated while the spectrum at 100 keV and above is hardly influenced (red curve). With lead shielding (green curve) the peaks and thus the sample information below 300 keV have disappeared. The two double peaks in the region of 80 keV are x-ray peaks originating from the lead shielding. To analyze the lead shielded samples, the "high-energy spectra" were used. Figure 3-5 shows the respective spectrum for the 96-19 configuration.

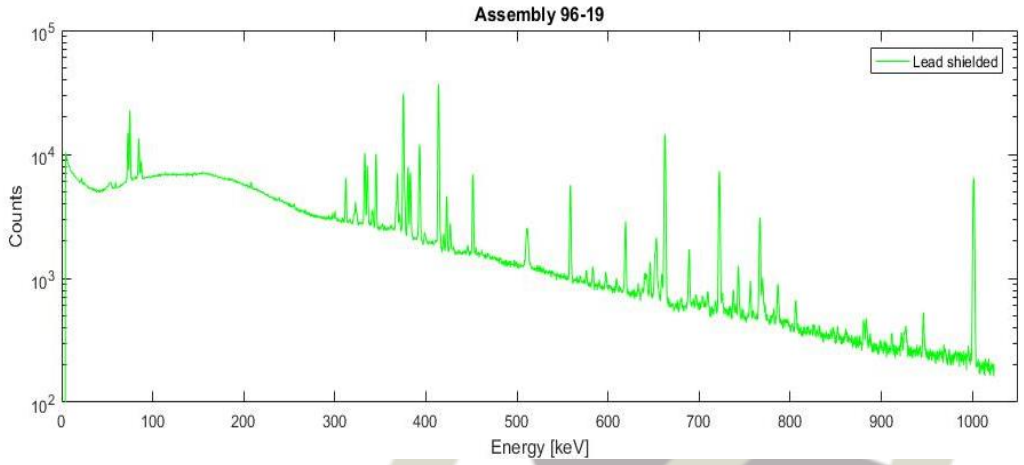

Figure 3-5. "High-energy spectrum" of the 96-19 assembly with lead shielding

Interpretation

The spectra were analyzed with FRAM and MGA codes to determine the isotopic compositions of plutonium, the respective time since chemical separation, and the isotopic composition of uranium for all three MOX assemblies. Figure 3-5 shows, representative of the three MOX assemblies, the ^{239}Pu content calculated from spectra taken of the unshielded (labeled bare), cadmium-shielded, and lead-shielded 79-19 assembly.

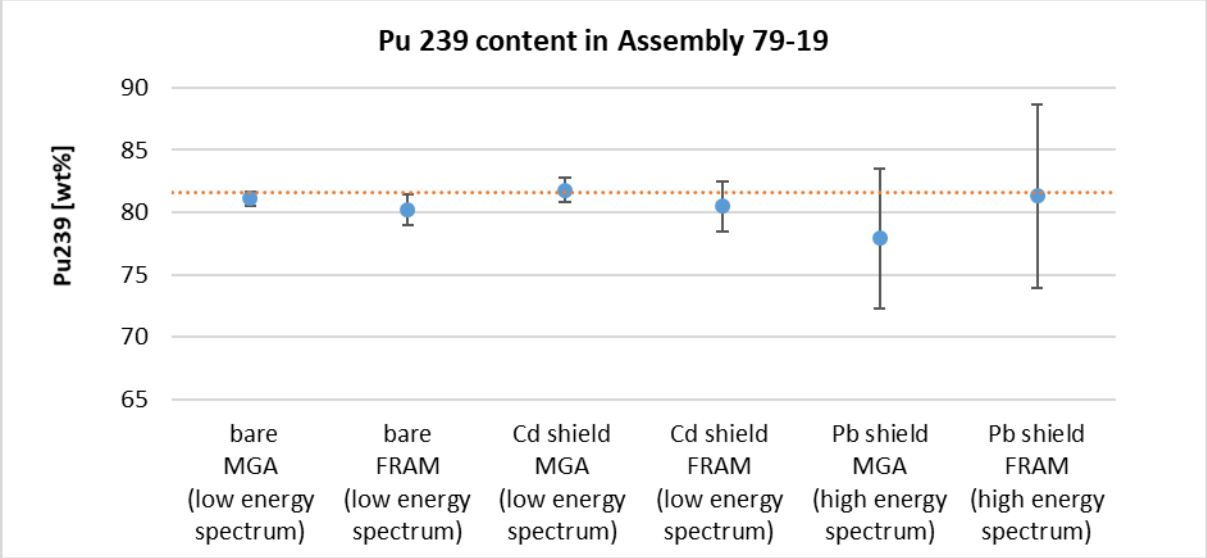

Figure 3-5. ^{239}Pu content in Assembly 79-19. Good agreement with measurement from SCK CEN, calculated to the reference date September 21, 2019 (dotted red line). Error bars show 2 σ values.

Figure 3-6 shows the time elapsed since chemical separation, determined for the 79-19 assembly. It is obvious, that with the lead shield used, an accurate determination of the "age" is not possible.

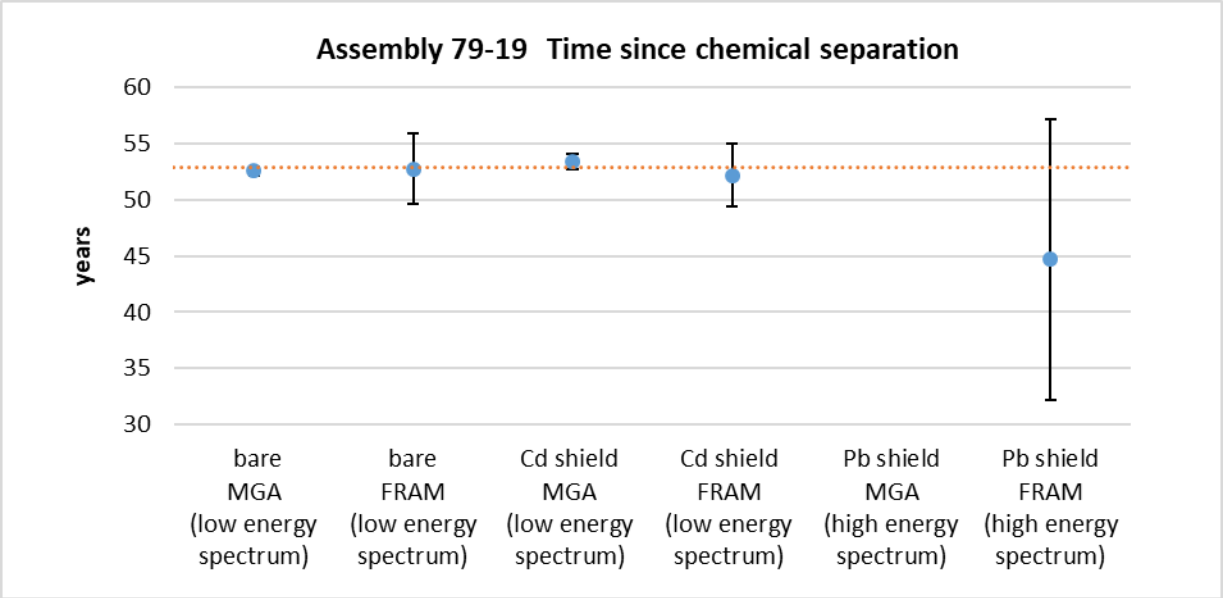

Figure 3-6. "Age determination" in Assembly 79-19, measured without shielding (labeled bare) and with Cd and Pb shieldings, respectively.

For unshielded and cadmium-shielded assemblies, the ^{235}U content in uranium can be determined. Figure 3-7 shows the results derived for the cadmium-shielded assemblies. A distinction between depleted, natural, and low-enriched uranium was possible.

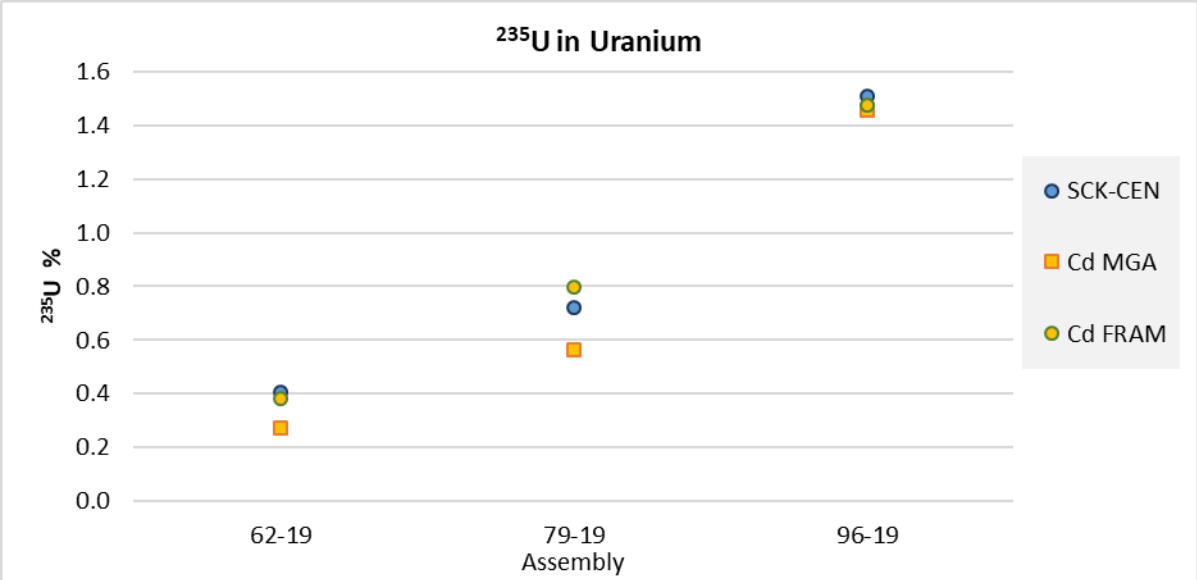

Figure 3-7. ^{235}U content in Uranium of the three MOX assemblies

3.1.3 Norway (IFE, DSA)

Introduction

The UK-Norway initiative (UKNi) has been investigating technologies and methodologies that could contribute to a future nuclear disarmament verification effort. A key project has been the development of an Information Barrier (IB), a system that is designed to verify a set of attributes assigned to a nuclear warhead, while not revealing the information that is being regarded as sensitive by the host party. To be useful, the host and inspecting party must have confidence that the IB does what it is specified to do (and nothing else). This sets strong requirements on the certification and authentication of the employed software and hardware.

The efforts of the UKNi-IB were centered around the automated analysis of a gamma-ray spectrum for attributes like the presence of plutonium and its ratio. For a plutonium-based nuclear warhead, the isotopic ratio of ^{240}Pu to ^{239}Pu is commonly assumed to be indicative of weapon-suitable material. The goal of the IB development is, therefore, to verify explicitly whether the isotopic ratio of an inspected item is below an agreed upon threshold, without revealing the total gamma-ray spectrum of the tested specimen.

The UKNi algorithm[7] for the isotopic ratio (^{240}Pu/^{239}Pu) has been tested on the IPNDV gamma-ray data. The results were compared and summarized with PC/FRAM[8] code.

Experimental Setup

A p-type coaxial HPGe detector (ORTEC GEM-30185) was connected to the data acquisition system using FAST ComTec MCA4, with 32k ADC resolution, to acquire the gamma-ray data from test samples. The test samples were MOX spent fuel arranged in hexagonal bundle. The gamma-ray spectra from two such assemblies with constant and varying plutonium content were collected. Experiments were performed with and without lead shielding (5 mm and 10 mm thick). In order to get better peak to Compton scattering ratio, a collimator was used on the crystal probe of the detector. A lead cylinder of 5 cm with an opening in the center of 3 mm was used as a collimator as shown in Figure 3-8. The algorithm[9] was applied to following data:

[7] Edward Day, *Information Barrier Software: Detailed Algorithm Overview*, Technical report, UKNi, Version 1.0.
[8] T.E. Sampson & T.A. Kelley, "PC/FRAM: A Code for the Nondestructive Measurement of the Isotopic Composition of Actinides for Safeguards Applications," *Applied Radiation and Isotopes* 48, no. 10-12 (1997): 1543–1548.
[9] Edward Day, *Information Barrier Software: Detailed Algorithm Overview*, Technical report, UKNi, Version 1.0.

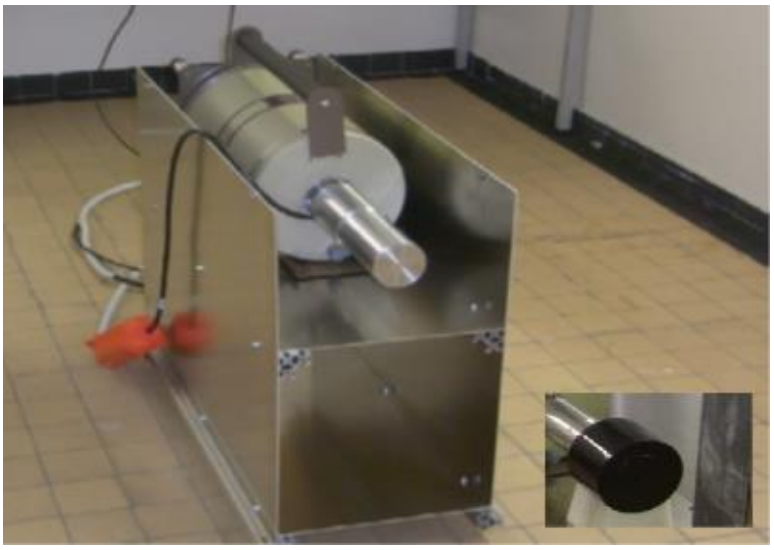

Figure 3-8. Experimental setup for gamma-ray detection (Source: SCK CEN. Used by permission)

- Raw decay gamma-ray data collected from fuel bundle containing 100 cm-long fuel pins with ^{239}Pu content ~ 62 %.
- Raw decay gamma-ray data collected from fuel bundle containing 50 cm-long fuel pins. This MOX fuel bundle had three different plutonium content, with the middle part having ^{239}Pu content ~ 96 %.

Analytical Method

UKNi-IB is designed to determine the presence of ^{239}Pu and the isotopic ratio of ^{240}Pu/^{239}Pu in a plutonium sample. An isotopic ratio of 0.1 has been chosen as reference level to verify the tested sample as "weapon-grade."

In our analysis we concentrate on the determination of the isotopic ratio from the gamma-ray spectra in the energy region 630–680 keV methodology that has been adopted, which is the same as described in the reference.[10] The algorithm[11] is implemented in C++ using the ROOT data analysis framework.[12] The main features of the UKNi algorithm are described under:

1. Calibrating the spectra using ^{152}Eu decay peaks at energies 121.782 keV and 77.904 keV. The IB system assumes a linear energy distribution between these two energies.
2. Identification and location of the centroids of ^{241}Am peak at 662 keV and of ^{239}Pu peak at 645.94 keV.
3. Calculating the average background at energies greater than 662 keV.

[10] N. Syed, S. Hustveit, O. Reistad & S. Siem, "Investigating the Method of UK-Norway Initiative Information Barrier," INMM 60th Annual Meeting Proceedings, California 2019.
[11] Edward Day, *Information Barrier Software: Detailed Algorithm Overview*, Technical report, UKNi, Version 1.0.
[12] R. Brun & F. Rademakers, "ROOT: An Object Oriented Data Analysis Framework," *NIM A* 389, no. 1–2 (April 1997): 81–86, doi: 10.1016/s0168-9002(97)00048-x.

4. Determining the full width half maximum (FWHM) of ^{241}Am peak at 662 keV. Assuming Gaussian distribution, the peak is calculated: $n_x = K_1 e^{K_2(x-c')^2} + b_x$, here
   n_x modelled count in channel x;
   K_1 normalization factor;
   K_2 Gaussian constant;
   x channel number;
   c' calculated location of centroid;
   b_x background in channel x.

   a. A χ^2 parameter is calculated for each channel: $\chi^2_x = \frac{(n_x - m_x)^2}{m_x}$, here n_x is the modelled count and m_x is the measured count in channel x.
   b. A χ^2_{red} is thus calculated for the peak region: $\chi^2_{red} = \frac{\sum \chi^2_x}{\nu}$, here, ν is the degrees of freedom.
   c. An optimized value of $\chi^2_{optimal}$ is estimated by calculating the χ^2_{red} of adjacent channels and selecting the lowest value.
   d. Since, $\chi^2_{optimal} = g(FWHM)$, the optimized FWHM gives the peak height of 662 keV.
   e. The final χ^2 value should pass two criteria, (i) $\delta\chi^2 < 0.001$ and (ii) $\chi^2 < 16$.

5. Using the same method as above χ^2_{red} is calculated for ^{239}Pu peak at 645.94 keV. However, FHWM is held constant and an optimal $\chi^2_{optimal}$ is calculated as a function of background continuum $\chi^2_{optimal645} = g(b_{645})$.
6. A multiplet incorporating the ^{239}Pu, ^{241}Am, and ^{240}Pu peaks is de-convoluted for 642.35 keV γ-ray photopeak. This is done by estimating the contributions from other nearby prominent peaks.
   a. The estimated contribution is given by: $n = \frac{I_{\gamma 637}}{I_{\gamma 645}} h_{645}\, e^{(x-c_{637})^2} + \frac{I_{\gamma 640}}{I_{\gamma 645}} h_{645}\, e^{(x-c_{640})^2} + \frac{I_{\gamma 641}}{I_{\gamma 662}} h_{662}\, e^{(x-c_{641})^2}$, here
      $I_{\gamma x}$ Emission probability at x keV;
      h_x Height of measured γ-ray photopeak at x keV;
      x channel number;
      c_x channel of centroid of modelled γ-ray peak at x keV;
   b. If m' is the remaining pulse height distribution once modelled peaks are subtracted: $m' = m - n$.
   c. χ^2_{red} value of our region of interest is evaluated and optimized.

7. The isotopic ratio, ^{240}Pu/^{239}Pu is derived using: $n = \frac{\left[\frac{h_{642} \cdot t_{1/2} \cdot (^{240}Pu)}{I_{\gamma 642}}\right]}{\left[\frac{h_{645} \cdot t_{1/2} \cdot (^{239}Pu)}{I_{\gamma 645}}\right]}$, where

   h_x net peak at x keV; and
   $t_{\frac{1}{2}}(^{y}Pu)$ half-life of Pu isotope.

Results and Discussion

The results of IB algorithm on IPNDV test samples are shown in Figure 3-9, Figure 3-10, Figure 3-11. The arrows indicate the peak values of the 645.96 keV ^{239}Pu and 662 keV ^{241}Am. The continuous red lines give the χ^2 minimized fit to the data and the dashed lines highlight the estimated background. The ^{240}Pu contribution to the multiplet at ≈ 642 keV is fitted after subtraction of the contribution by ^{239}Pu and ^{241}Am and the whole resulting multiplet is drawn with the dashed green line.

The method has previously been successfully tested on PIDIE (Plutonium Isotopic Determination Inter-comparison Exercise) plutonium samples and plutonium test samples. At IPNDV test campaign, it has been observed that background radiation and count rate was high. This put a limitation on the throughput of measured gamma-ray spectra, as the detector dead time was observed to be high. This led to relatively low data statistics at region of interest in a given time.

The multiplet peak at 640 keV gamma-ray energy region is more prominent in 50 cm long fuel assembly spectra then the one in 100 cm-long fuel assembly gamma-ray spectra.

The above-mentioned spectra were also tested with the commercially available code PC/FRAM[13] to analyze and determine the plutonium content of the IPNDV test samples. The results are summarized in Table 3-1. The best determined ^{239}Pu content is ~ 91.13% for the 50 cm-long fuel assembly with no absorber as compared to PC/FRAM giving 93.15% given ^{239}Pu content of 96 %. Similarly, best estimated ^{239}Pu content ~ 62.86 for the 100 cm-long fuel assembly with no absorber as compared to PC/FRAM giving 55% and given value of ^{239}Pu 62%.

The investigation on the deviations of determined isotopic ratio using UKNi methods in comparison to the given nominal values is still underway.

[13] T.E. Sampson & T.A. Kelley, "PC/FRAM: A Code for the Nondestructive Measurement of the Isotopic Composition of Actinides for Safeguards Applications," Applied Radiation and Isotopes 48, no. 10-12 (1997): 1543–1548.

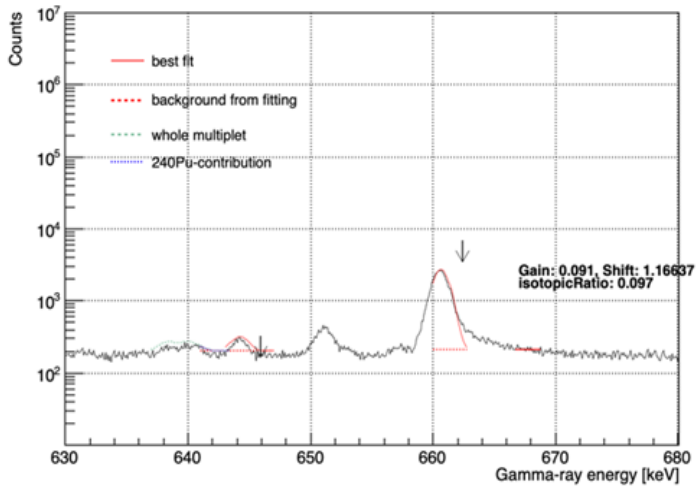

Figure 3-9. UKNi algorithm applied on 50 cm-long fuel assembly with no absorber

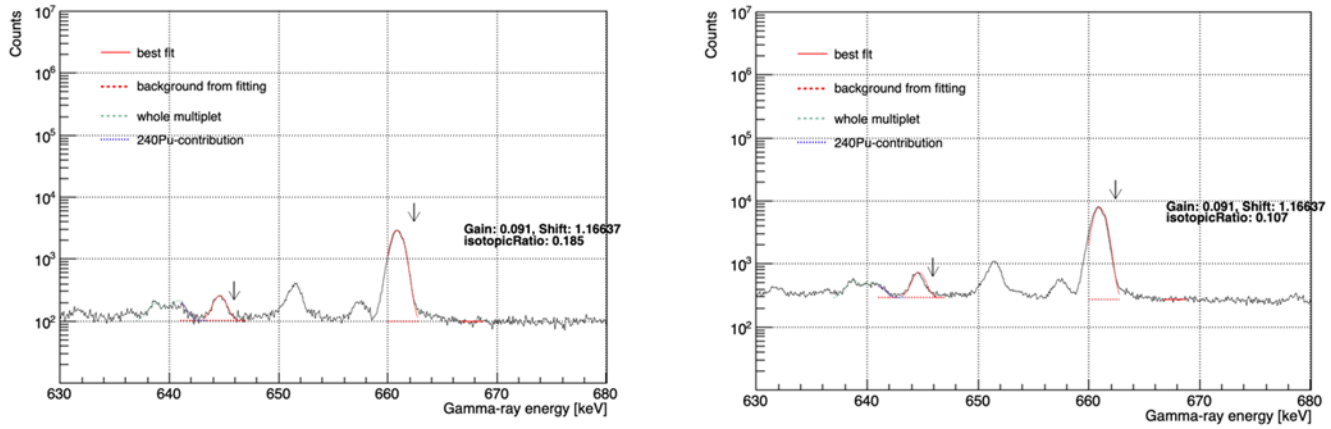

Figure 3-10. UKNi algorithm applied on 50 cm-long fuel assembly with 5 mm and 10 mm Pb absorbers, respectively

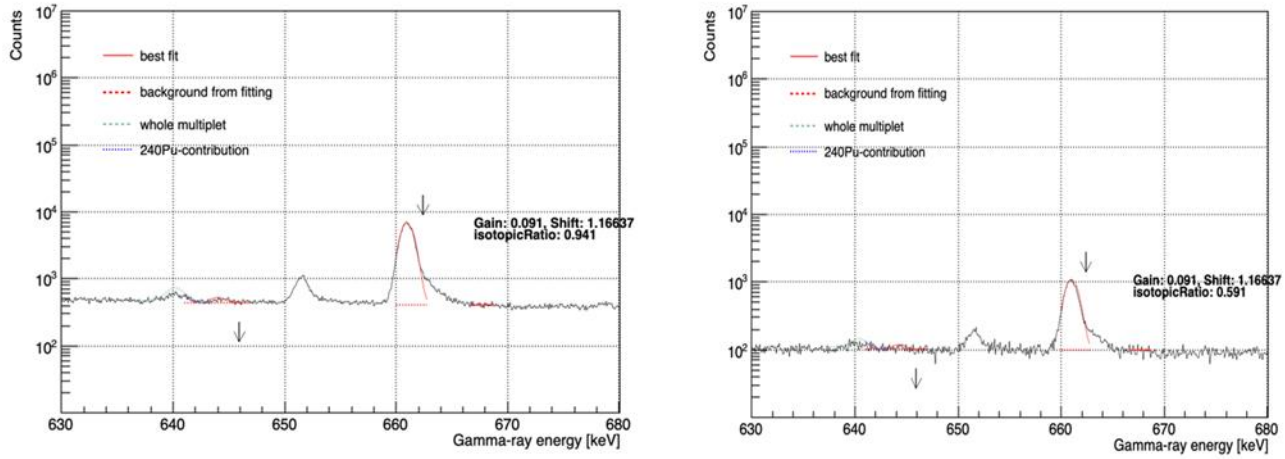

Figure 3-11. UKNi algorithm applied on 100 cm-long fuel assembly with 5 mm Pb absorber and no absorber, respectively

Test Fuel Assembly (FA)	Isotopic Ratio ($^{240}Pu/^{239}Pu$)	^{239}Pu %	
	UKNi	PC/FRAM	UKNi
50 cm long FA with 5 mm lead absorber	0.185	-	84.37 %
50 cm long FA with 10 mm lead absorber	0.107	91.62 %	90.34 %
50 cm long FA with no absorber	0.097	93.15 %	91.13 %
100 cm long FA with 5 mm lead absorber	0.941	74.78 %	51.51 %
100 cm long FA with no absorber	0.591	55 %	62.86 %

Table 3-1. Isotopic ratio determination using UKNi method and PC/FRAM method

3.1.4 Hungary (Centre for Energy Research)

Applied Technology

Detector: Canberra GL 2020 planar HPGe detector, liquid nitrogen cooled (Figure 3-13)

20 cm^2 surface 2 cm thickness crystal

Very Good Resolution And Efficiency In 30 Kev–300 Kev Range

Quite Good efficiency in 300 keV–1200 keV range

Analyzer: Ortec DigiDart portable, compact, battery-operated MCA (16 k-channel)

Softwares: Ortec Gamma-Vision data collection code

Canberra MGA evaluation package

Others: Homemade adjustable height rack for the detector

Led collimator with different aperture

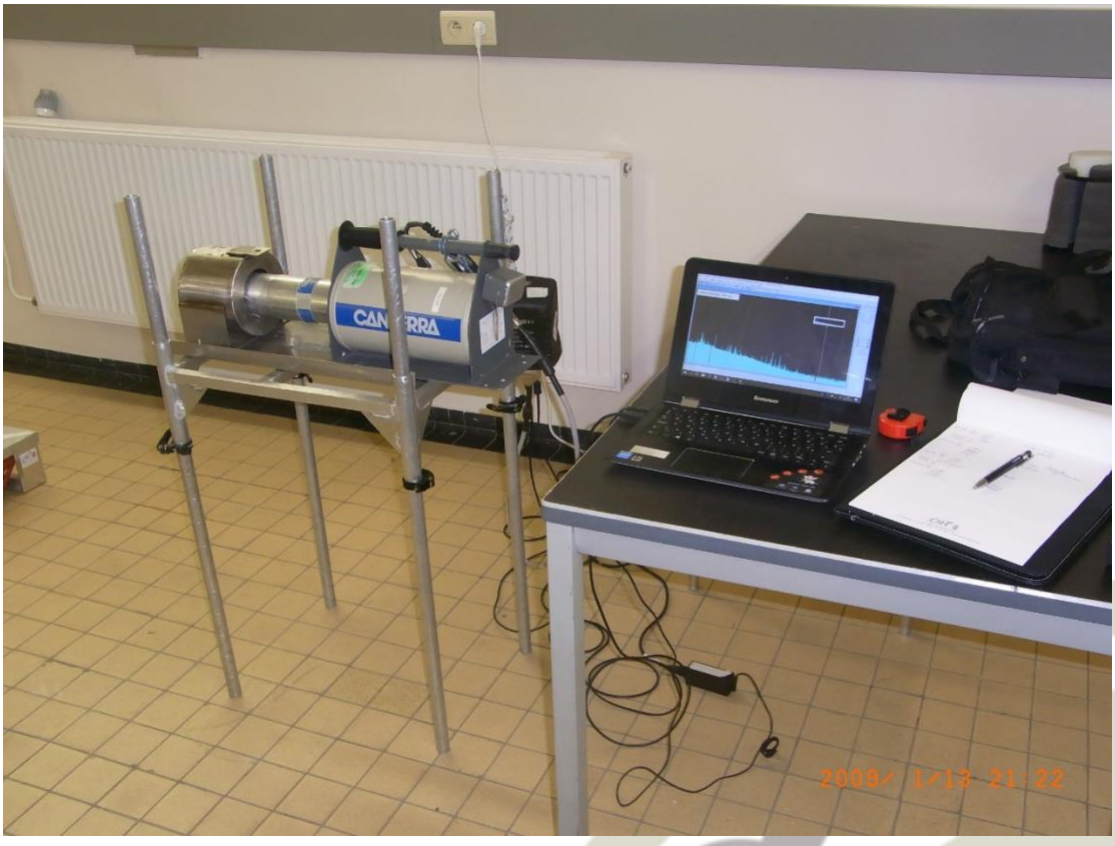

Figure 3-12. Measurement setup (Source: SCK CEN. Used by permission)

Measured objects: T1 79% ^{239}Pu isotopic ratio plutonium content MOX assemblies

T2 79% + 96% ^{239}Pu isotopic ratio MOX

T4 62% ^{239}Pu isotopic ratio Pu content MOX

Applied shieldings on the assemblies:

NONE

5 mm Pb

5 cm PE

1 mm Cd

Spectra were collected mainly from 130–150 cm distance except in the case of lead shielded assemblies (30–35 cm) and the "scanner" mode with the narrow collimator.

The measurement times were as long as the important peaks had reached the necessary precision for the evaluation (300–5000 s)

The MGA analysis were taken on all spectra. We got excellent results for the plutonium isotopic composition ^{241}Am contents and the production date in all cases except the led shielded samples (Table 3.2).

Type	Measured distance (cm)	Measured height (cm)	Kolli dia (mm)	LT (s)	^{238}Pu (%)	^{239}Pu (%)	^{240}Pu (%)	^{241}Pu (%)	^{242}Pu (%)	^{241}Am (%)	Age (Years)
Type 1 (79% ^{239}Pu)	150	47	100	925	0.06	81	18	0.25	0.5	2.8	52
1 mm Cd	150	47	100	964	0.05	84	16	0.26	0.3	2.5	49
5 mm Pb	150	47	100	2411	None						
Type 2 (79+96% ^{239}Pu)	130	47	100	362	0.04	90	10	0.14	0.0	1.4	49
	130	57	100	693	0.03	89	11	0.13	0.0	1.5	52
	20	57	22	1058	0.01	96	4	0.02	0.0	0.2	50
	20	75	22	906	0.06	82	17	0.24	0.4	2.6	51
1 mm Cd	60	57	100	925	0.03	90	10	0.12	0.0	1.3	50

10 mm PE	130	57	100	880	0.03	88	12	0.14	0.1	1.6	52
5 mm Pb	35	57	100	4747	none						
Type 4 (62% ^{239}Pu)	140	80	22	784	1.05	69	25	1.91	3.0	8.1	34
1 mm Cd	140	80	100	629	1.07	68	26	1.91	3.2	8.2	34
5 mm Pb	30	80	100	970	none						

Table 3-2. Summary of the obtained results

Lessons Learned

Without shielding or with polyethylene shielding the MGA evaluation works well.

The cadmium shielding could help for the evaluation, cutting the low-energy backscattering.

The measurement can detect and differ the reactor grade (RG) and weapon grade (WG) plutonium content. The detection limit is not determined in this phase. When the equipment is used in “scanner mode” (narrow collimator or slit collimator) the different plutonium-isotopic composition areas could be detected, similarly to the gamma-camera.

In the case of heavy metal shielding (lead or depleted uranium), the MGA evaluation is impossible because of the missing peaks in the 30–300 keV region, but there are visible peaks for different plutonium isotopes and ^{241}Am above 300 keV.

Conclusion

The method used by our team cannot be applied to the original warhead, due to the heavy metal sphere outside of the WG plutonium.

The method can be applied for presence and absence measurement of nuclear material in the 14th step of dismantlement, when the materials are separated.

The RG and WG materials could be discriminated in the same container.

3.2 Medium-Resolution Detectors

3.2.1 Belgium (SCK CEN)

The goal of the measurement was to verify the performance of the Cadmium Zinc Telluride detector (CZT) with respect to their capabilities in verifying SNM with or without shielding. More specifically, we looked at sensitivity to nuclear material amount, radionuclide composition, and shielding.

Detector and Setup

We carried out medium resolution gamma-ray measurements between 0–1600 keV with a 10 mm × 10 mm × 5 mm quasi-hemispherical CZT detector[14] with a preamplifier embedded in the detector head from Ritec. The detector had a resolution, expressed as full width at half maximum, of 1.3% at 661 keV.[15] The weight of such a device is about 100 g and is operated at room temperature. The data acquisition was done with an MCA527 from GBS-Elektronik coupled to a laptop computer. The high voltage was also supplied by the MCA527.

Pictures of the measurement setup are shown in Figure 3-13. All measurements were carried out with a 1.1 mm Cd shielding around the fuel assembly to limit the count rate due to the 60 keV gamma-ray line of ^{241}Am and most of them without a lead collimator. The measurement times were between 20–120 minutes with a distance between 0–25 cm. The distance was chosen to limit the dead time to less than 5%.

Figure 3-13. Setup of the measurement with the CZT detector: (left) a Cd shielding covers the assembly; (right) the Pb collimator can be seen in between the detector and the assembly (Source: SCK CEN. Used by permission)

[14] Spectrometric Detection Probe with Large Volume CdZnTe Detector SDP 500 (S), Operator's Manual, Ritec (2013).

[15] A. Borella, M. Bruggeman, R. Rossa &P. Schillebeeckx, "Peak Shape Calibration of a Cadmium Zinc Telluride Detector and Its Application for the Determination of Uranium Enrichment," *Nuclear Instruments and Methods A* 986 (2021) 164718, https://doi.org/10.1016/j.nima.2020.164718.

Measured Samples

The measured samples consisted of the hexagonal bundles, *96–19, 79–19,* and *62–1, with 62–19* and *62–61* measured at the mid position. In addition, the *96–19* was measured at the bottom position where the ^{239}Pu relative content is 79%$_{wt}$. We indicate this measurement as *96–19 bottom*. The bundle *62–61* was also measured with 5 cm CH_2 and 10 mm Pb shielding. These two measurements were carried out also with a lead collimator.

Analysis and Results

Because traditional gamma-ray spectroscopy approaches are not yet mature for medium-resolution detectors,[16] this technology was tested to see if qualitative information could be obtained in terms of being able to discriminate weapon- or civil-grade plutonium, sensitivity to the sample mass and shielding. Rather than aiming at determining the net peak areas of complex and/or overlapping peaks, we looked at how ratios of net counts in defined region-of-interests (ROI) change with respect to a given reference baseline. The ROI was selected to include strong peaks of radionuclides of interest (e.g., ~ 100, 208, 335, 414, 662, and 723 keV). In all, the ROIs ^{241}Am peaks are present except for the ROI at around 414 keV, which should be little affected by ^{241}Am.

Spectra

The left of Figure 3-14 shows the obtained spectra for the *96-19*, *79-19*, and *62-19* bundles. The right of Figure 3-14 compares the detector response obtained with CZT with the one obtained with LEGe detector. The worse energy resolution results in peak overlapping.

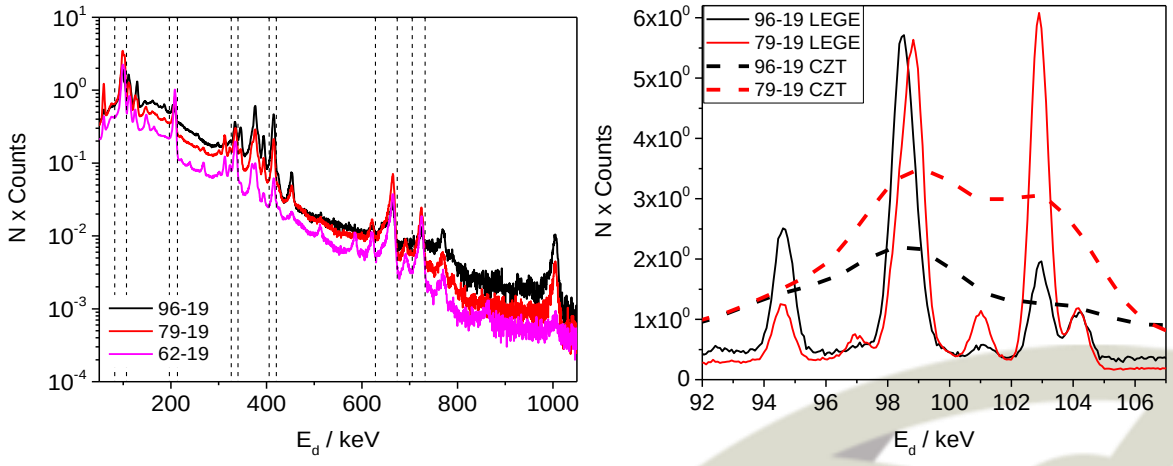

Figure 3-14. (left) Spectra measured with the CZT detector for the three bundles; (right) Comparison of the detector response around the 100 keV region with LEGe and CZT detectors.

[16] Proceedings of the International Workshop on Isotopic Analysis of Uranium and Plutonium by Nondestructive Assay Techniques for Nuclear Safeguards (Vienna: IAEA, February 16–19, 2021).

ROI Ratio Analysis

We determined the background subtracted counts $C_{i,j-k,m}$ for different ROI and fuel types.

The background of each ROI was determined by linear interpolation using the average spectral values over three channels before and after the beginning and end of the ROI, respectively.

The indexes *i*, *j*, *k,* and *m* have the following meaning:

- *i* identifies the ROI (approximatively corresponds to the energy of the ROI in keV).
- *j-k*, indicates the bundle where
  - *j* indicates the fuel type.
  - *k* number of pins (1, 19, and 61).
- *m* indicates the type of shielding and collimator (Cd, CH_2+Pb, Cd+coll, CH_2+Pb+coll).

The ROI were chosen around 100, 208, 335, 414, 662, and 723 keV.

Change in ROI with Respect to Mass

For the *62* fuel assembly with 1, 19, and 61 pins, measured with cadmium and without collimator, the following quantity was determined:

$$\alpha_{i,62-k,Cd} = \frac{C_{i,62-\mathrm{k},Cd} \Big/ C_{i,62-1,Cd}}{C_{723,62-k,Cd} \Big/ C_{723,62-1,Cd}}$$

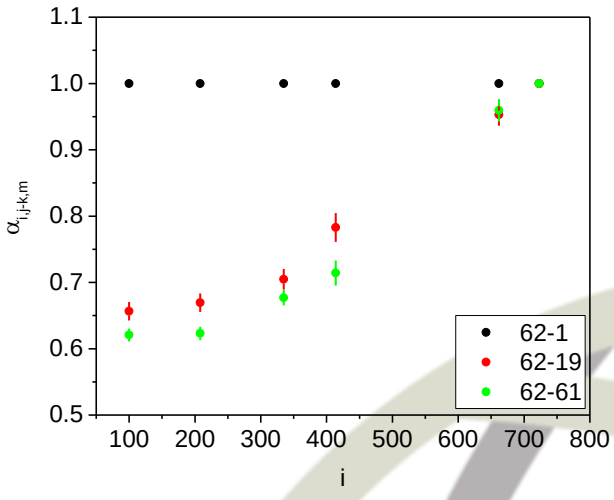

Figure 3-15. The $\alpha_{i,j-k,m}$ dependence on *i* (energy) and *k* (mass) when fixing *j* (type/composition) and *m* (shielding/collimator).

In this way $\alpha_{i,62-1,Cd}$ equals 1 for every *i* and the trend of $\alpha_{i,62-k,Cd}$ can indicate a change in the detection efficiency due to a different mass and therefore a different self-absorption with

respect to the reference (1 pin) (Figure 3-16). Given the different number of pins the geometry and therefore the self-absorption and the solid angle seen by the detector are also different. This phenomenon comes into play in the observed trend of $\alpha_{i,62-k,Cd}$.

Change in ROI with Respect to Composition

We considered the fuel bundles *96-19*, *79-19*, and *62-19* measured with a cadmium shield and without collimators and determined the parameter α with the equation below. The *96-19* bundle was measured also in the bottom position.

$$\alpha_{i,j-19,Cd} = \frac{C_{i,j-19,Cd} \Big/ C_{i,96-19,Cd}}{C_{723,j-19,Cd} \Big/ C_{723,96-19,Cd}}$$

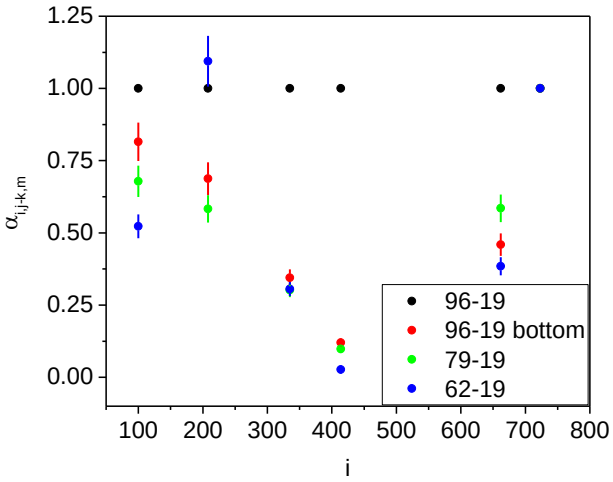

Figure 3-16. The $\alpha_{i,j-k,m}$ dependence on *i* (energy) and *j* (type/composition) when fixing *k* (mass) and *m* (shielding/collimator).

In this way $\alpha_{i,96-19,Cd}$ equals 1 for every *i* and the trend of $\alpha_{i,96-19,Cd}$ can indicate a change in the detector response due to a different composition with respect to the reference (*96-19* in the mid-position) (Figure 3-17).

The data for the *96-19* bottom and *79-19* cases should agree within the uncertainties although the composition for the two cases is not identical due to a slightly different plutonium content and uranium enrichment, which could impact the results.

Given the high content ^{241}Am, the different ^{241}Am content may come into play when looking at different composition. The fact that the ROI at 414 keV should be not affected by ^{241}Am and that we see large deviation from the baseline is an encouraging indication that the deviation is due to the different ^{239}Pu content.

Change in ROI with Respect to Shielding and Collimation

We considered fuel *62-61* with 61 pins and determined for all shielding/collimation types:

$$\alpha_{i,62-61,m} = \frac{C_{i,62-61,m} / C_{i,62-61,Cd}}{C_{723,62-61,m} / C_{723,62-61,Cd}}$$

Although the impact of the collimator is within 15%, the shielding attenuates the response down to zero and exhibits a trend different from the one observed when mass and composition change.

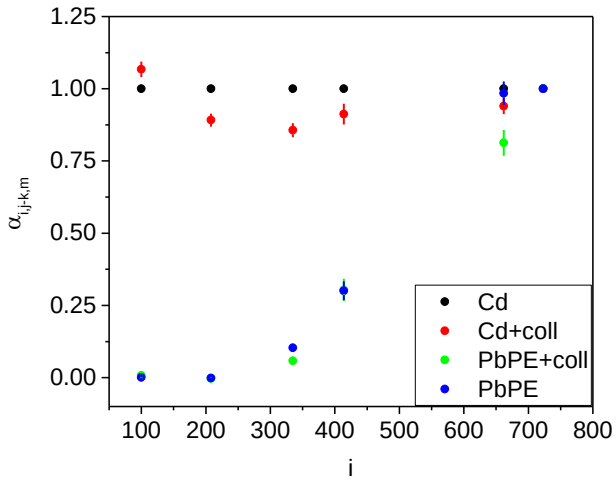

Figure 3-17. The $\alpha_{i,j-k,m}$ dependence on *i* (energy) and *m* (shielding/collimator) when fixing *j* (type/composition) and *k* (mass).

The data with PE (5 cm) and Pb (10 mm) shielding indicate that the signatures above 350 keV start to become visible (Figure 3-18). The use of a collimator is recommended to improve the peak to background below 300 keV and limit the influence of a non-uniformly space distributed gamma source (e.g., axial profile, other sources in the room). However, when looking at the $\alpha_{i,j-k,m}$ the impact due to the collimator does not seem to be significant for the considered cases.

The impact of the lead shielding is characterized by a different trend with energy when compared with the observed trends due to different mass/composition.

All Data

So far, we analyzed subsets of data where only one characteristic (composition, shielding, mass) was changed. Now we consider all spectra together to see if the characteristics (composition, shielding, mass) can be identified by studying $\alpha_{i,j-k,m}$. The reference was the 96 mid fuel and $\alpha_{i,j-k,m}$ was defined as:

$$\alpha_{i,j-19,Cd} = \frac{C_{i,j-19,Cd} \Big/ C_{i,96-19,Cd}}{C_{723,96-19,Cd} \Big/ C_{723,96-19,Cd}}$$

Grouping all data together reveals that it is not evident to distinguish the influence of composition, mass and shielding/collimator, although it is possible to identify ROI ratios who are more sensitive to variation in the material type. The data at 414 keV seem to be sensitive to the relative plutonium content only. The trend due to the lead shielding is still clearly present. The sensitivity to the mass is not evident and requires further study possibly of the ROI at around 100 and 208 keV (Figure 3-19).

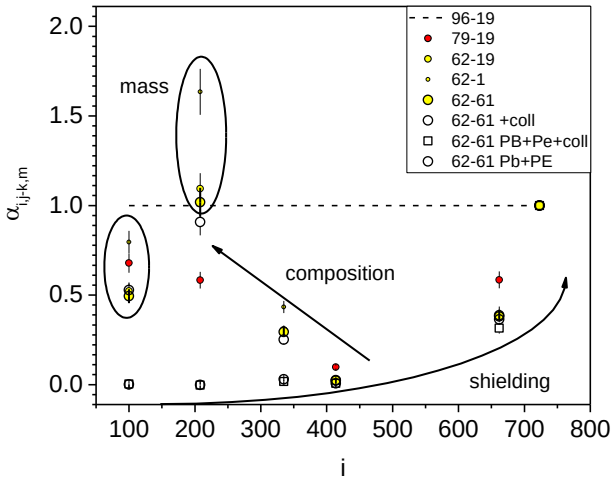

Figure 3-18. The $\alpha_{i,j-k,m}$ dependence on *i* (energy), *j* (type/composition), *k* (mass) and *m* (shielding/collimator).

Conclusions

We considered a CZT detector as non-destructive assay technology for disarmament verification. Although traditional spectra analysis tools are not available for complex spectra, we proposed a simplified data analysis approach based on ROI ratios. The obtained results revealed that ROI ratios are sensitive to mass and composition changes when there is a priori knowledge about the composition and amount of material, respectively. The presence of shielding can be inferred from the energy dependence of the count rate when compared to an unshielded case.

The measurement time is in the range of 30–120 minutes, which is probably too long for verification inspections. Considering larger detector could reduce the measurement time.

The fact that CZT detectors can be operated at room temperature and are of compact size makes them suitable to be used as so-called radiation template. In this sense a “template” provides a unique set of (radiation) signatures used to provide confirmatory verification of an

inspectable item against a 'trusted' item's reference data set."[17] We could verify that the method is geometry- and background-dependent and affected by the decay of radionuclides, which then should be accounted for.

One could argue that because the spectra currently cannot be analyzed with "traditional" methods, they do not necessitate an information barrier. However, "the radiation template of classified or sensitive items must be protected."[18]

3.2.2 Japan (JAEA)

Configurations

- Sample
  - 62 w/o ^{239}Pu: 1 pin, 19 pins, 61 pins
  - 79 w/o ^{239}Pu: 19 pins
  - 62 w/o ^{239}Pu: 19 pins
- Shielding: Bare bundle, Pb: 10 mm; Cd: 2 mm; PE: 50 mm
- Measurement Distance: 40 cm from center of MOX bundle (Detector photo
- Figure 3-19)
- Measurement time:
  - 90 min (^{239}Pu: 62 w/o, 1 pin, bare)
  - 60 min (^{239}Pu: 62 w/o, 61 pins, Pb shielded)
  - 20 min (others)

[17] Technology data sheet NM9, "Radiation Templates," WG3 IPNDV, May 15, 2017.
[18] Ibid.

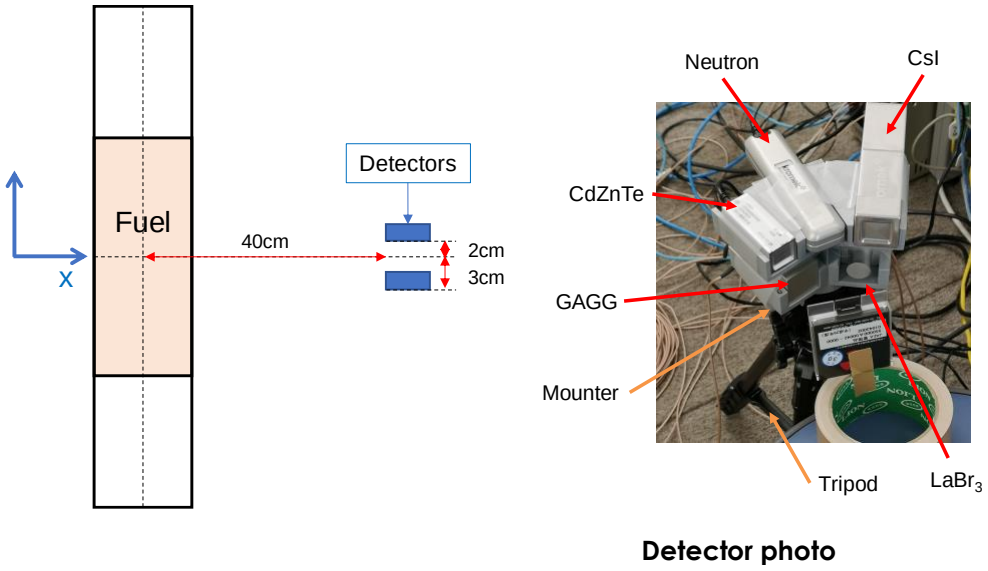

Figure 3-19. Experimental setup (Source: SCK CEN. Used by permission)

Detector Specifications

Name	Detector type	Detector size	Energy resolution @662 keV	DSP/MCA
Techno-AP XGG2080	GAGG ($Ce:Gd_3Al_2Ga_3O_{12}$)	25 × 25 × 25 mm	< 10%	Techno-AP APV8102-12 (12 bit)
Techno-AP XL-050I	$LaBr_3$	12.7 mmD × 12.7 mmL	< 3.5%	Techno-AP APV8102-12 (12 bit)
Kromek SIGMA50	CsI(Tl)	1x1 × 2in.	< 7.2	Built-in (12 bit)
Kromek GR1-A+	CZT	10 × 10 × 10mm	< 2.0%	Built-in (12 bit)

Table 3-3. Detector specifications.

Results and Discussion

Medium-resolution detector can be deployed for presence/absence measurement of plutonium and could likely to be used for plutonium grading.

- CsI(Tl) and GAGG are unfeasible for plutonium measurement due to low energy resolutions (>7% FWHM @662 keV).
- CZT (<2.0% FWHM @662 keV) and $LaBr_3$ (<3.5% FWHM @662 keV) have enough lower resolution for ^{239}Pu detection, but ^{240}Pu peaks cannot be identified (Figure 3-20).

- Calibration curve on ^{239}Pu amount can be drawn for the bare bundle with the CZT and $LaBr_3$. Lower detection (LD) limit of ^{239}Pu is a several tens of grams with the CZT (<50g ^{239}Pu) and $LaBr_3$ (<100g ^{239}Pu) small detectors with 20-min measurement for the bare MOX bundle (Table 3-4).
- LD in ^{239}Pu amount could not be evaluated for lead shielded MOX bundle with 20-min measurement due to low statistics.
- Plutonium grading by ^{240}Pu /^{239}Pu activity ratio is not possible with the CZT and $LaBr_3$ (medium-resolution detectors), because ^{240}Pu peak cannot be recognized.
- Pu grading by ^{241}Am /^{239}Pu ratio could likely be performed with the CZT (

- Figure 3-21) and $LaBr_3$ (medium-resolution detectors), but it's required the initial amount of ^{241}Am contained in the SNM and SNM age for accurate grading.

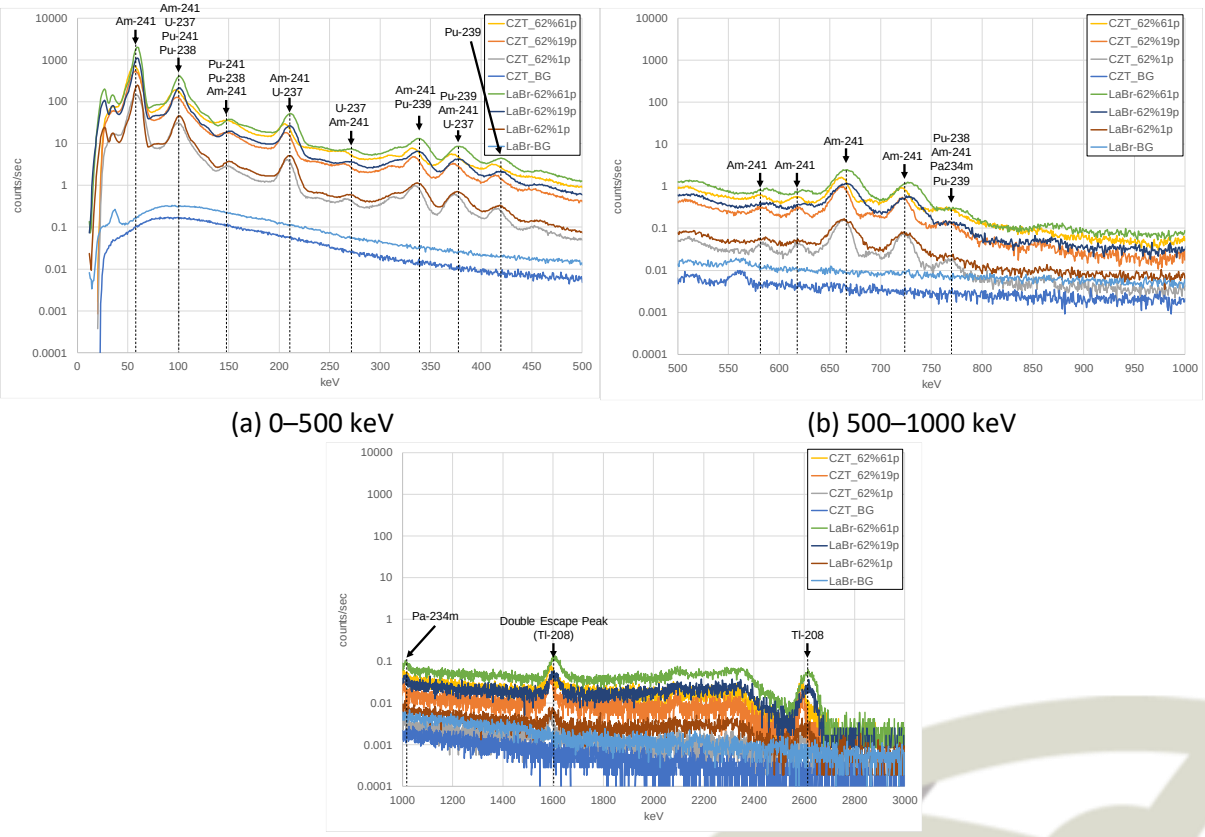

(a) 0–500 keV

(b) 500–1000 keV

(c) 1000–3000 keV

Figure 3-20. Peaks in measured spectrum by CZT and $LaBr_3$ detectors (bare bundle, ^{239}Pu: 62 w/o)

^{239}Pu, w/o	pins	^{239}Pu, g	Time, s	CZT		$LaBr_3$	
				LD, cps	LD, g(^{239}Pu)	LD, cps	LD, g(^{239}Pu)
96	19	222.3	20	0.31	30.1	0.64	41.6
79	19	218.5	20	0.64	32.2	0.73	43.0
62	1	42	60	0.22	29.5	0.31	56.9
62	19	798	20	1.68	40.1	1.48	36.8
62	61	2562	20	2.64	49.1	2.55	84.7

Table 3-4. Lower detection limit in ^{239}Pu (bare bundle)

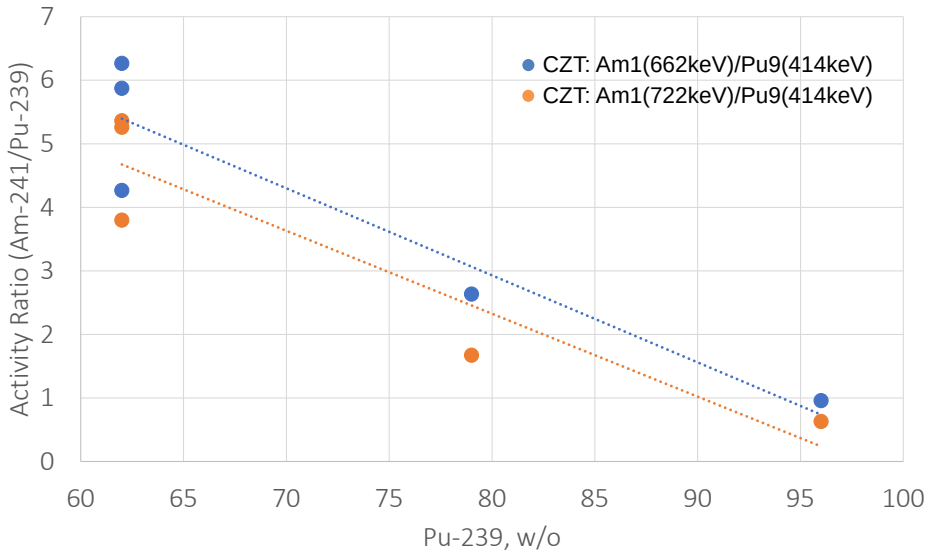

Figure 3-21. ^{241}Am /^{239}Pu activity ratios estimated based on the measured gamma-ray spectrum by the CZT detector

3.2.3 United Kingdom (Ministry of Defence, AWE)

Our objective was to use well-established neutron and gamma detectors with an aim to measure validation data from a well-known source to aid modeling for treaty verification and to allow testing of verification algorithms.

We measured 19 fuel pins from both the 79% and 96% ^{239}Pu fuel compositions using both gamma and neutron detectors. Table 3-5 summarises the six configurations used. The two fuel pin sets were measured with three different shielding configurations: no shielding; Cd 2 mm thick; and a shielding of Pb, 10 mm thick, over PE, 50 mm thick.

79% ^{239}Pu Fuel Pins	96% ^{239}Pu Fuel Pins
No Shielding	No Shielding
Cd (2mm)	Cd (2mm)
Pb (10mm) and PE (50mm)	Pb (10mm) and PE (50mm)

Table 3-5. Six shielding configurations used by the UK during this measurement campaign

During the Belgium Measurement Campaign, the UK fielded two mechanically cooled HPGe detectors (Detective EX-100 and Transpec 100T) and one sodium iodide (NaI) Identifinder detector

For gamma measurements, the results from both HPGe detectors were not useable due to damage to equipment in transit. The NaI results for both the 79% ^{239}Pu Fuel and 96% ^{239}Pu fuel for all configurations can be seen in Figure 3-22. These measurements were taken over a short time span of 5 minutes at a distance of 128 cm from the center of the fuel bundle. The NaI measurements were taken on a table with a height of approximately 75 cm, which was approximately 20 cm from a wall.

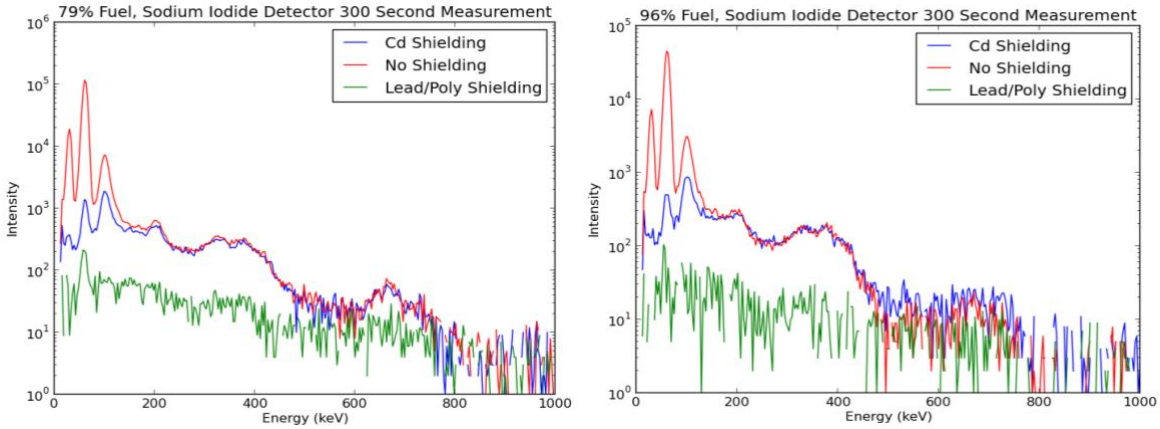

Figure 3-22. Results from NaI detector for the 79% ^{239}Pu fuel in the left figure and 96% ^{239}Pu fuel in the right figure. The y axis is the total counts per channel.

Although the results from the NaI detector are not as useful as high-resolution HPGe spectra for exact isotopic identification, there are other uses for lower-resolution spectral measurements such as this in a verification system. One such use could be in *radiation signature template matching*.

If a treaty defines two different classes of object (or "treaty accountable item"), then an effective verification regime will require the ability to distinguish between these two classes. For example, if a site were declared to contain objects of type "79% ^{239}Pu" and of type "96%

^{239}Pu," how can we be sure that an item declared to be one type is not, in fact, the other? What if the gamma spectrum is considered sensitive information and cannot be viewed by inspectors? This presents an opportunity to use a template matching method, and it can be done using the low-resolution gamma data obtained during this campaign. The NaI low-resolution data can be re-binned around energy groups of interest that correspond to isotopes of interest for the class of objects. A spectral measurement of a known object can then be saved as a "template" and compared against the spectra from subsequent objects, using a statistical metric to determine the likelihood of the spectra being from the same type of object. In this method, the potentially sensitive spectra of the template and the subsequent objects never need to be revealed to the inspector, only the statistical result of the comparison.

Figure 3-23 shows an example using two sets of NaI data taken during the campaign for this template matching. Table 3-6 shows the results of a comparison for all the data taken during the measurement campaign by the UK. The spectra are compared using a reduced chi-square metric, with a value less than four indicating a match between the template and object spectra. This shows the ability to easily distinguish between things that are classed as a match (on the diagonal) and things that are not classed as a match to the template spectrum. It also shows that in this case the presence of shielding would affect whether something was deemed to belong to the correct class.

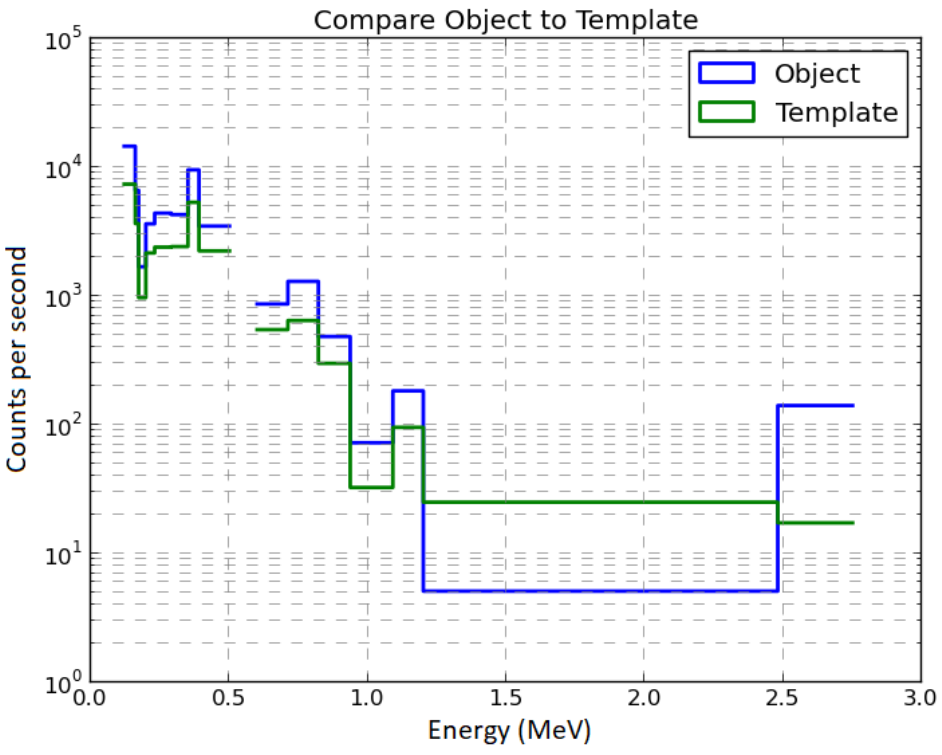

Figure 3-23. Example of the comparison over re-binned energy groups between a template and object

OBJECT	TEMPLATE					
	79% No shielding	79% Cd shielding	79% Pb PE shielding	96% No shielding	96% Cd shielding	96% Pb PE shielding
79% No shielding	0.22	57.45	12631.86	91.68	309.36	52194.9
79% Cd shielding	15.54	0.25	5935.5	67.35	58.14	29942.56
79% Pb PE shielding	82.67	79.05	0.28	71.58	65.45	150.5
96% No shielding	26	31.74	3375.32	0.23	46.73	15405.73
96% Cd shielding	32.93	19.02	1611.89	17.46	0.22	9406.58
96% Pb PE shielding	92.33	90.8	32.9	86.35	84.26	0.41

Table 3-6. Template verification using low-resolution gamma spectra. The table values are the reduced chi-square statistic for the object spectrum compared to the template. Green, low values indicate a good match. Red, high values indicate a large difference between the two measurements.

3.2.4 Canada (Canadian Nuclear Laboratories (CNL))

Introduction

The ability to verify the presence/absence of nuclear material inside closed container is of great importance to nuclear disarmament verification (NDV). Techniques such as passively counting and characterizing neutrons and gamma-rays emitted by fissionable materials (FM), including SNM, could be used to for that purpose. Most FM isotopes exhibit a low rate of radioactive decay and spontaneous fission. For example, the spontaneous fission neutron yields from ^{235}U and ^{238}U are 2.99×10^{-4} $n \cdot s^{-1} \cdot g^{-1}$ and 1.36×10^{-2} $n \cdot s^{-1} \cdot g^{-1}$ respectively.[19] These low emission rates combined with self-absorption and low detection efficiency of typical counting systems lead to weak and statistically poor response signals relative to background. This makes detection using passive neutron and gamma techniques difficult. In addition, detection will be much more difficult if a tamper that acts as shielding is present around the fissile core.

[19] N. Ensslin, "Chapter 11: The Origin of Neutron Radiation," In D. Reilly, N. Ensslin & H. Smith Jr. (Eds.), *Passive Nondestructive Assay of Nuclear Materials* (Washington, DC: Office of Nuclear Regulatory Research – U. S. Nuclear Regulatory Commission, 1991): 337–356.

Experiments at SCK CEN in Belgium aimed to assess the usefulness of a high-detection efficiency neutron and gamma-rays counting systems for application in NDV. Task included collecting gross neutron count rate, Rossi-Alpha distribution (coincidence measurements), and gamma spectra from several nuclear fuels with various shielding around. Table 3-7 lists the specific samples measured along with the configuration of the measurement system. As show in Figure 3-24, both neutron and gamma-ray data were taken simultaneously.

^{239}Pu % (Isotopic)	Number of Pins	Sample Total Mass (kg)	^{239}Pu Mass (kg)	Configuration
62	1	0.5	<0.1	1. No shielding
62	19	10.2	0.8	2. No shielding
62	61	32.8	2.6	3. No shielding
				4. 5 mm Pb
				5. 50 mm PE (CH2)
				6. 50 mm CH_2 + 10 mm Pb
				7. Cd shielding; He3 inside High Density Polyethylene (HDPE)
				8. Cd shielding; He3 outside HDPE
				9. No Shielding; He3 outside HDPE
79	19	6.2	0.2	10. No shielding
96	19	6.2	0.2	11. No shielding

Table 3-7. Configurations explored during SCK CEN campaign for IPNDV technology demonstration

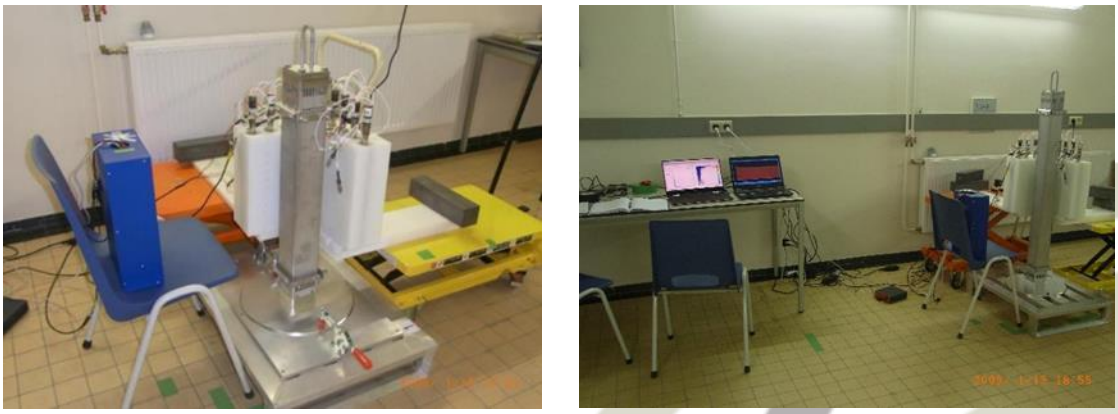

Figure 3-24. Experimental setup for neutrons and gamma-rays measurements at SCK CEN (Source: SCK CEN. Used by permission)

Gamma-Ray Techniques: Gross Counting and Spectroscopic Modes

For the gamma-ray measurements, two commercial mid-resolution gamma detectors were used: one based on NaI, and the other on CLYC crystals. Figure 3-25 presents gamma-rays spectrum for configuration 11 (sample with 96% of ^{239}Pu). Due to mid-resolution capability of the gamma detectors, results are combination of peaks originating from uranium and plutonium isotopes as well as from ^{241}Am. The resolution of both systems was not good enough, and therefore we were not able to identify peaks due to plutonium or uranium. The relatively intense gamma signal from ^{241}Am is strong making mid-resolution gamma detectors (NaI and CLYC) non-useful for identification of plutonium and uranium. More analysis is required to use these detectors, and collimators may be required for gamma measurements depending on the sample's activity.

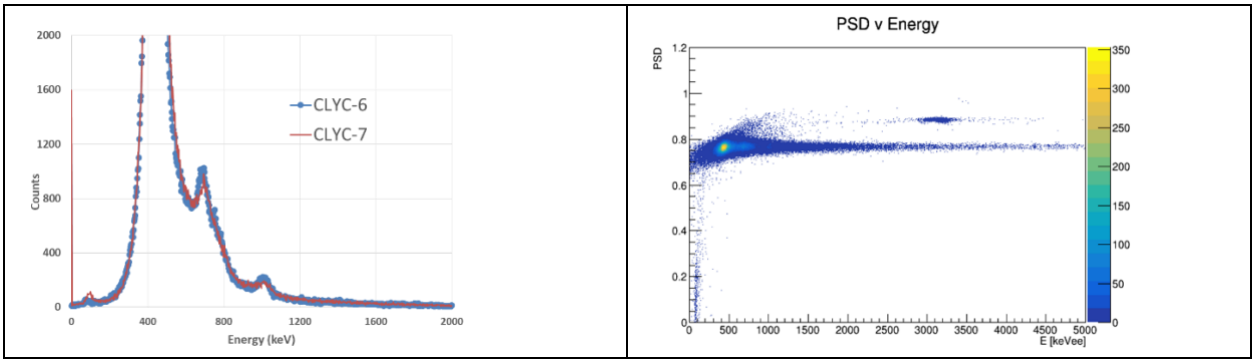

Figure 3-25: (left) Gamma-ray spectra for configuration 11 (sample with 96% of ^{239}Pu); (right) pulse shape discrimination (PSD) for CLYC-6

4 Neutron Measurements

4.1 Neutron Counters

4.1.1 Belgium (SCK CEN)

Neutron coincidence counting allows estimating the mass of a sample containing SNM provided that the radionuclide vector is known.[20] This technology was used to verify its ability to determine the mass of the available SNM and determine its performance with respect to shielding material and limit of detection.

The technology measures the time correlation between events measured with neutron detectors. In addition to the total count rate *T*, the reals rate *R* is determined from the number

[20] A. Borella et al., "*Neutron Coincidence Measurements and Monte Carlo Modelling of Waste Drums Containing Reference Nuclear Material,*" proceedings of the 2021 ANIMMA Conference.

of detected neutrons in two time windows that are opened every time a neutron is detected. *R* is a measure of the amount of material emitting neutrons by spontaneous fission.

In the proposed approach, we apply Hage's point model[21] to determine the intensity of the spontaneous fission (SF) source term and detection efficiency. From the spontaneous fission source term, it is possible to determine the ^{239}Pu mass by knowing the isotopic composition of the sample (e.g., from gamma-ray spectrometry).

Detector and Setup

Two WM3400 slab counters[22] were deployed. The sample to be assayed is placed between the detectors as shown in Figure 4-1.

Totals, "R+A," and "A" are measured with a JSR-12 shift register.[23] Each detector is equipped with a shift register. The logical "OR" of the signals are also processed by a shift register as well as an MCA527 from GBS-Elektronik with upgraded firmware.[24] The upgraded firmware allows saving the time stamps of the detected events for an offline analysis to determine the distribution of correlated events. By considering the two detectors as a whole, one limits the impact of possible asymmetrical detector arrangements.

Figure 4-1. Measurement setup for the neutron coincidence counters (Source: SCK CEN. Used by permission)

[21] D.M. Cifarelli & W. Hage, "Models for a Three-Parameter Analysis of Neutron Signal Correlation Measurements for Fissile Material Assay" *Nuclear Instruments and Methods A* 251 (1986): 550–563.
[22] Model 3400 Slab Neutron Counter Hardware Reference Material, Canberra Industries Inc., 2009.
[23] Model JSR-12 Neutron Coincidence Analyzer User's Manual, Canberra Industries Inc., 2006.
[24] MCA527 for Neutrons, https://www.gbs-elektronik.de/media/download_gallery/mca527_neutron.pdf. Last accessed 19/04/2018.

Measured Samples

All five assemblies (*96–19, 79–19, 62–1, 62–19, 62–61*) were measured. All measurements were conducted with 1.1 mm Cd around the fuel assembly. For fuel types *79–19* and *96–19*, the measurements were also conducted without cadmium. The fuel type *96–19* was also measured with 5 cm CH_2 around the assembly and 1.1 mm thick Cd sheet on the detector, as well as with 5 mm Pb around the assembly and 1.1 mm thick Cd sheet on the detector.

Measurements were done at two distances, 26 cm and 95 cm, from the outer surface of the assembly. The measurement time depends on the neutron emission of the sample and was either 1800 s or 3600 s. The uncertainty on the reals rate R was about 2% at 26 cm distance and about 5–10% at 96 cm.

Analysis and Results

The data analysis reported here considers only the ORed response of the two slab counters measured with the MCA527.

For the *96–19* assembly, there was less impact due to (α,n) reactions, both totals and reals were insensitive to cadmium, and almost insensitive to Cd+Pb (5% reduction on the totals), with CH_2+Cd the totals were attenuated by 30% and the reals by 43%.

In all, the cases the uncorrelated background was relatively high with the ratio A/(R+A) ranging from 88.4% (96-19 with PE+Cd shielding) to 99.8% (*62-61* with Cd, at 1 m distance). In the worst case, the reals rate could be determined with a relative uncertainty of 8%.

The equations of the Hage's point model equations in absence of multiplication

$$T = F_S \nu_{s1} \varepsilon (1 + \alpha) \qquad (1)$$

$$R/f = F_S \nu_{s2} \varepsilon^2 \qquad (2)$$

are solved being *T* and *R* the measured observables. In the equations ε is the detection efficiency, α is the ratio between the neutron emission due to (α,n) reaction and spontaneous fission, F_S the number of fission per seconds, ν_{s1} and ν_{s2} are the first and second factorial moment of the distribution for the neutron emission through spontaneous fission. The die-away of the system was measured with a ^{252}Cf source (55.3±1.0 μs) and the gate occupation factor *f* was then calculated as indicated in Ref. [21].

We used the composition from the fuel specifications to solve the equations; the α term in the Eq. 1 is determined from the composition and nuclear data of the fuel. We derived the calculated F_S source term and, from the radionuclide composition, the total mass of heavy metal was then calculated.

The obtained ratio between the calculated mass of heavy metal and the nominal one from the fuel specification for different cases and as a function of the mass of heavy metal mass is shown in Figure 4-2.

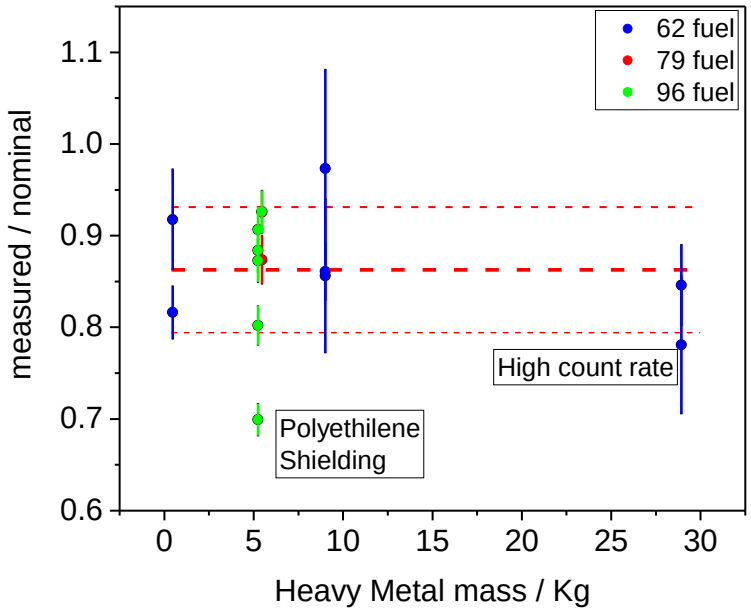

Figure 4-2. Ratio between the measured and nominal sample mass for different assemblies and configurations.

The results show an average underestimation of the mass by about 14%. The fact that the multiplication factor is not accounted for can explain the observed bias as well as the fact that the conditions to apply the point model were not fully met. The two outliers are recorded for measurement with polyethylene shielding and for high count rate. In the case of high count rate, the dead time has a potential impact on the observable and was not yet accounted for. In the case with polyethylene shielding a correction factor for multiplication in the assembly may be needed when solving the point model equations.

Conclusions

The results indicated that measurements were challenging due to the very high (α,n) background. Such a background component is not expected to be present in verification scenario. With such unfavourable conditions we could detect ~20 g of $^{240}Pu_{eq}$ at 1 m distance in 30 minutes.

The limit of detection is however influenced not only by the (α,n) component but also on the accuracy on the background induced by neighbouring items and cosmic rays induced spallation in lead or high Z material.

Despite the fact that the conditions to apply the point model equations were not fully met, relatively good results in terms of estimation of the total mass were achieved. The determination of the mass with the point model approach requires the knowledge of the radionuclide composition to the determine the relative contribution (α,n) to spontaneous fission in the source term.

Being sensitive to spontaneously fissioning material is a signature very difficult to spoof; therefore, the measurement of the reals rate can be used to detect absence/presence of spontaneously fissioning material whether with aim of quantifying the mass (with isotopics) or a quick verification of items.

4.1.2 Japan (JAEA)

Configurations

- Sample
  - 62 w/o ^{239}Pu: 1 pin, 19 pins, 61 pins
  - 79 w/o ^{239}Pu: 19 pins
  - 62 w/o ^{239}Pu: 19 pins
- Shielding: Bare bundle, Pb: 10 mm; Cd: 2 mm; PE: 50 mm
- Measurement Distance: 40 cm from center of MOX bundle (Detector photo
- Figure 4-3)
- Measurement time:
  - 90 min (^{239}Pu: 62 w/o, 1 pin, bare),
  - 60 min (^{239}Pu: 62 w/o, 61 pins, Pb shielded),
  - 20 min (others)

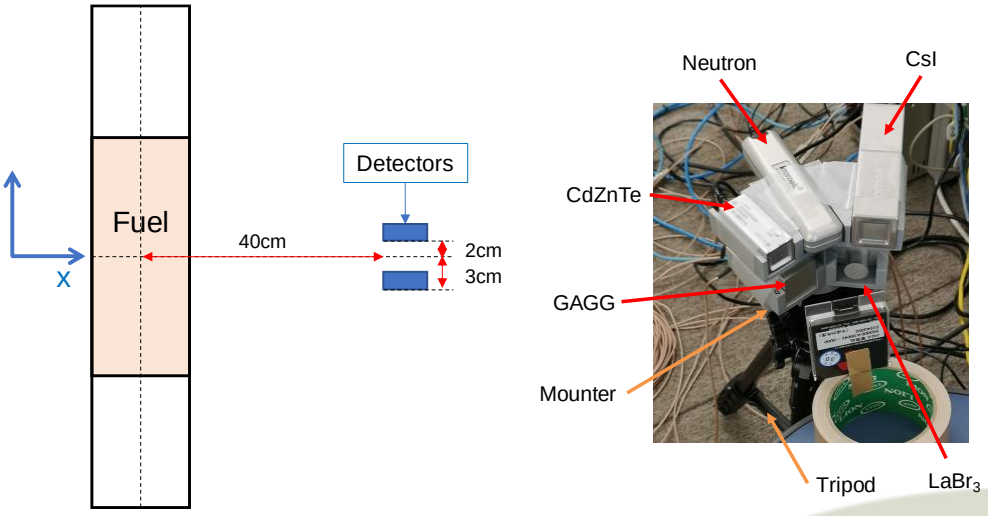

Figure 4-3. Experimental setup (Source: SCK CEN. Used by permission)

Detector Specifications

- Name: Kromek TN15
- ^{6}LiZnS detector is used with SiPM photo-sensor. Equivalent to 100 mmL × 13 mmD He-3 (4 atm), >50% thermal neutron sensitivity

Results and Discussion

Small, single neutron counter can be deployed for plutonium absence/presence measurement (the present device has linear response to number of neutron source). Mass of plutonium metal could be estimated if plutonium isotopic composition data can be obtained by another device like passive gamma-ray spectrometer.

- Linear response to number of source neutron was observed in all the shielding conditions (self-shielding is much smaller than gamma-ray).
- Calibration curve on source neutron could be drawn for all shielding conditions (Figure 4-4). LD limit of WG-Pu metal was estimated as several hundreds of grams (roughly ten times higher than small-medium resolution gamma detectors, Table 4-1 and Table 4-2).
- Categorization of WG/RG plutonium is impossible by single neutron counting.

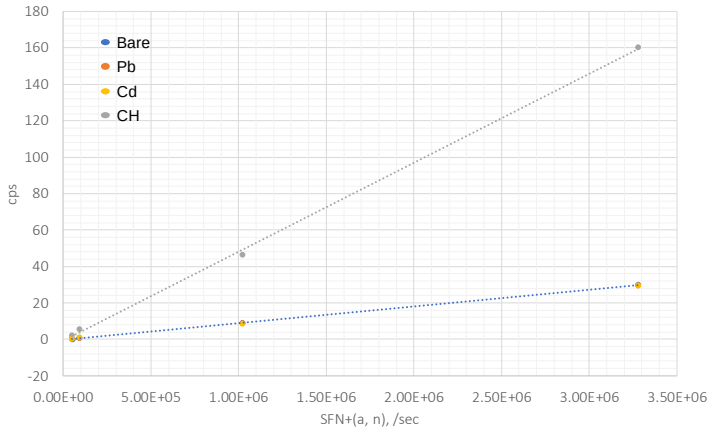

Figure 4-4. Calibration curve on source neutron

Shielding	LD, g Pu (SFN+(α,n))		
	96 w/o	79 w/o	62 w/o
Bare	427	253	7.80
Pd	328	194	6.00
Cd	313	185	5.70
PE	114	67.5	2.10

Table 4-1. Limit of Detection in g of Pu with 5 min measurement

Shielding	LD, g-Pu (SFN)		
	96 w/o	79 w/o	62 w/o
Bare	705	506	19.5
Pd	542	389	15.0
Cd	517	371	14.3
PE	188	135	5.21

Table 4-2. Estimated Limit of Detection in in g metal-Pu amount with 5 min measurement

4.1.3 United Kingdom (Ministry of Defence, AWE)

During the Belgium Measurement Campaign, the UK fielded three helium-3 (^{3}He) based neutron detectors (Nuclear Diagnostics Neutron Detector, or $(ND)^2$). The $(ND)^2$ is a ^{3}He-based, rugged, portable, and established detector, developed at Atomic Weapons Establishment (AWE). Each detector consists of four tubes of He^3 surrounded by high-density polyethylene—we fielded three panels stacked vertically for the neutron measurements, as shown in Figure 4-5. The detector measures thermal neutrons, both gross counts and list mode data.

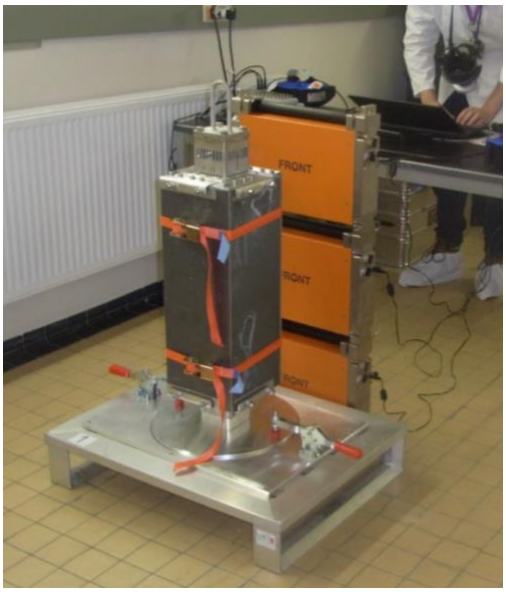

Figure 4-5. The $(ND)^2$ detectors in-field. Source: SCK CEN. Used by permission.

The gross count results from the $(ND)^2$ can be found in Table 4-3. The measurements were taken 30 cm from the source with a measured background rate of 68.7 counts per second (cps). Measurement time ranged between 30–85 minutes. The 79% ^{239}Pu fuel pins have significantly more neutron counts than the 96% ^{239}Pu fuel pins, for any of the shielding configurations. As expected, the lead and polyethylene shielding configuration causes a significant reduction in gross counts for both fuel pin types.

	79% ^{239}Pu Fuel (cps)	96% ^{239}Pu Fuel (cps)	MCNP Model of 79% Fuel	Error (%)
No shielding	958.36	395.74	1078.86	12.6
Cd shielding	968.01	414.33	1103.98	14.0
Pb and PE shielding	769.6	319.48	804.1	4.48

Table 4-3. Background subtracted simple neutron count results obtained using the $(ND)^2$ and MCNP modelled results for 79% ^{239}Pu fuel with difference to the experimental value (%)

The use of modeling is inevitable when planning for treaty verification. By using a detector response function for the $(ND)^2$, the Belgium experimental set up can be modeled. Using well-documented data, such as that from this campaign, for validation gives confidence in models which may be used for verification purposes in future. Table 4-3 shows the good comparison found between a model using MCNP and experimental data for the 79% ^{239}Pu fuel pins.

4.1.4 Canada (CNL)

The neutron counting system (NCS) system consists of several ^{3}He thermal neutron detectors that are interspersed throughout a polyethylene moderator. The system is adjustable and can be positioned on a platform to accommodate any size and shape of sample. Neutrons are counted using an MCA-527 multi-channel analyzer from GBS Elektronik, which is capable of measuring count rate and also creating a Rossi-Alpha spectrum in real time.

By comparing the neutron count rate for configurations with the ^{3}He detectors shielded and unshielded, one can qualitatively assess the neutron energy spectrum. As shown in Figure 4-6, for sample with 62% of ^{239}Pu, the count rate drops significantly when a bare ^{3}He detector is used, indicating the presence of fast neutrons. As shown in Figure 4-7, neutron count rates are linearly proportional to ^{239}Pu mass of the sample (left) and are confirmed to originate from a fission source by observing the typical Rossi-Alpha distribution (right).

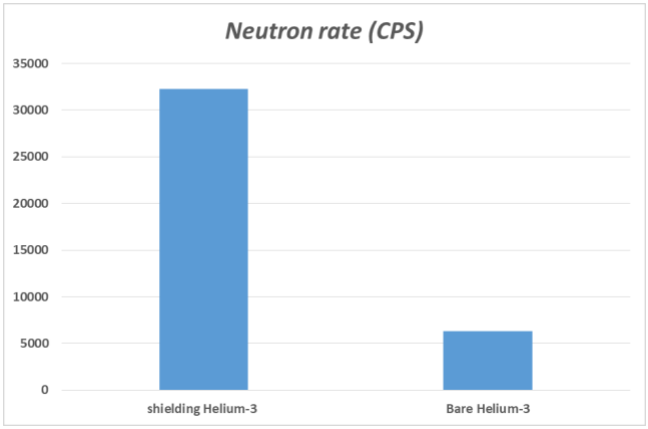

Figure 4-6. Neutron count rate as measured by shielded and bare ^{3}He from sample with 62% of ^{239}Pu

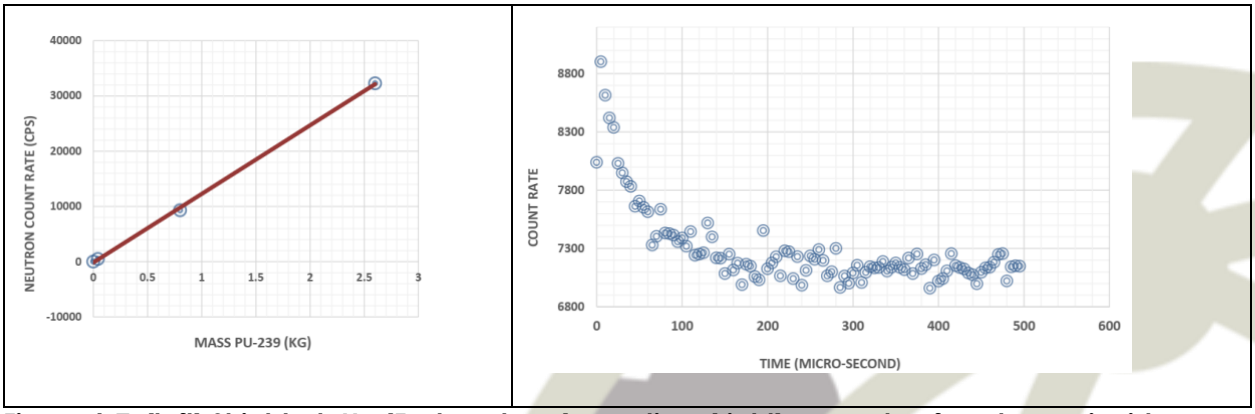

Figure 4-7. (left) Shielded ^{3}He (Fast neutrons) counting; (right) example of neutron coincidence and Rossi-Alpha distribution for configuration 3 with 62% of ^{239}Pu

Figure 4-8 shows neutron count rate for different shielding configurations around the sample. Count rate is observed to increase when lead or cadmium shielding materials are used. We suspect this due to gamma-rays generated by interaction of fast neutrons with these shielding materials, which leads to pile-up providing signals above threshold.

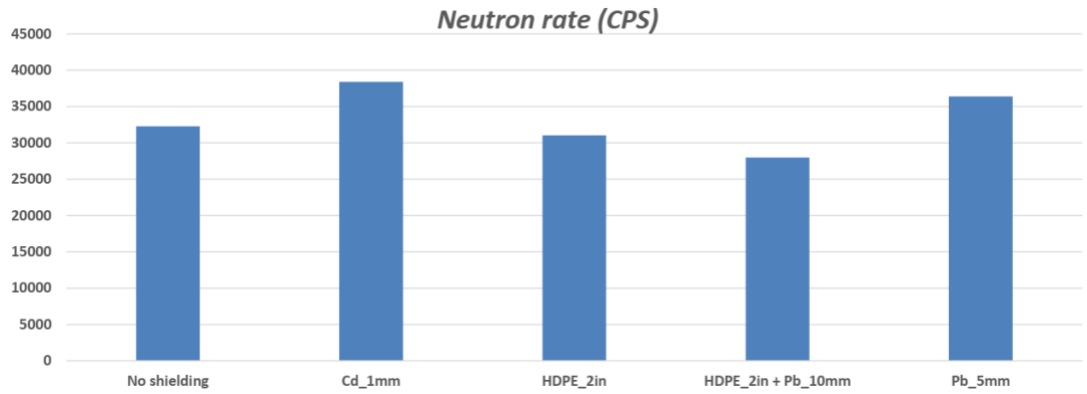

Figure 4-8. Neutron count rate for different shielding configurations

The neutron and gamma techniques were able to confirm presence of NM. The observed high neutron count rate eliminates uranium as main component of NM, and comparison with measurements done at CNL suggests the samples contain significant portion of plutonium. Mid-resolution detectors were not able to confirm isotopic composition

There are tentative long-term plans to perform Geant4 simulations to understand neutron counting in simple and coincidence mode. Particularly, we want to focus on understanding the increase in count rates when shielding materials are present, and for quantifying mass of SNM.

4.1.5 Hungary (Centre for Energy Research)

Applied Technology

Detector: Symetrica blades made for portal monitor

Analyzer: PTR-32

Software: PTR-32 written by J. Huszti

Modeling: MCNP 6.1

The neutron detectors and parts of the electronics were taken out of the two Symetrica portal monitor crates. The aim of a series of measurements including the IPNDV tests and the Monte Carlo modeling belonging to the investigations was to study the possibilities of those detectors beyond their original purpose.

The sensitive parts are ^{6}LiF doped scintillators followed by wavelength shifting and photoelastic modulators. The original electronics were used for pulse shape discrimination. The formed pulses of each detector were introduced into the separate channels of the PTR-32. The

sensitivity of each detector was calibrated previously. Two configurations of detectors were applied, as illustrated in Figure 4-9:

- **B:** The 2 blocks were placed one behind the other. The neutrons arrive perpendicular to the plane of the detectors. The detector blades are separated and surrounded by PE moderators.
- **C:** The detectors surround the fuel assembly, each blade is put in a separate moderator block, the neutrons arrive perpendicular to the plane of the detectors.

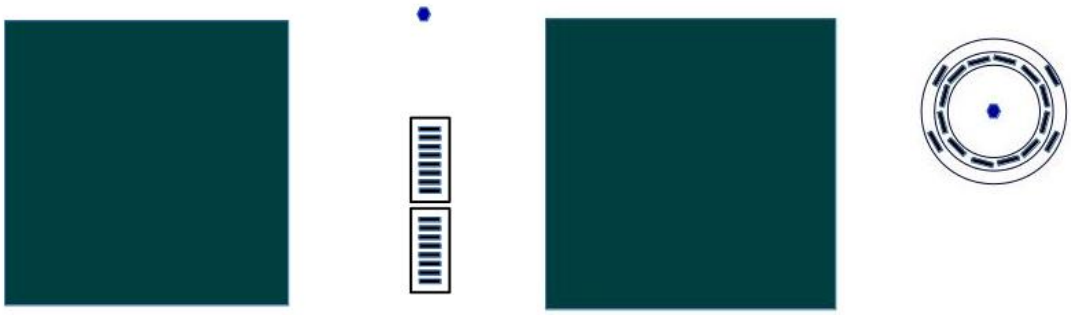

B C

Figure 4-9. Measurement configurations

Configuration B

As the neutrons pass through the detector system, they are moderated and captured. As a result, the thermal and epithermal neutrons are mostly captured in the first few blades, the higher energy neutrons are captured in the deeper layers.

The shields provided were not thick enough to completely absorb the emitted neutrons so we could demonstrate the presence of the fissile material even in the case of the weakest sources (19 pins, 96 % ^{239}Pu and 1 pin, 62 % ^{239}Pu fuel assemblies) with the strongest shielding. The measurements were conducted at high background in the vicinity of a large, shielded RaBe source. Under those circumstances the count rate measured for 19 pins, 96 % ^{239}Pu fuel assembly shielded by polyethylene and cadmium (weakest source) was the double as for the background.

The application of shields modified the neutron energy spectra. The measured response functions (count rate vs. channel number) reflected those changes (Figure 4-10). The polyethylene shield moderates the neutrons, which cause a count rate loss in channels 1-15 and a gain in channel 0. Subsequent cadmium shield causes a sharp drop in channel 0 and has no influence for channels 2-15.

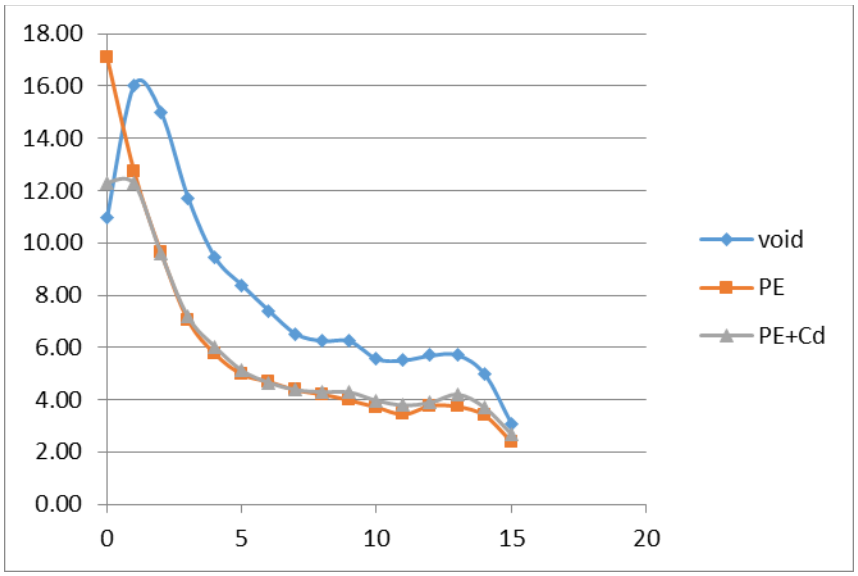

Figure 4-10. Measured response functions in different configurations

Unfolding of the energy spectra is in progress. This configuration of detectors also gives a possibility for the directional sensitivity. Figure 4-11 illustrates the response function vs. incoming angle as determined by MC simulation for two blocks of eight blades:

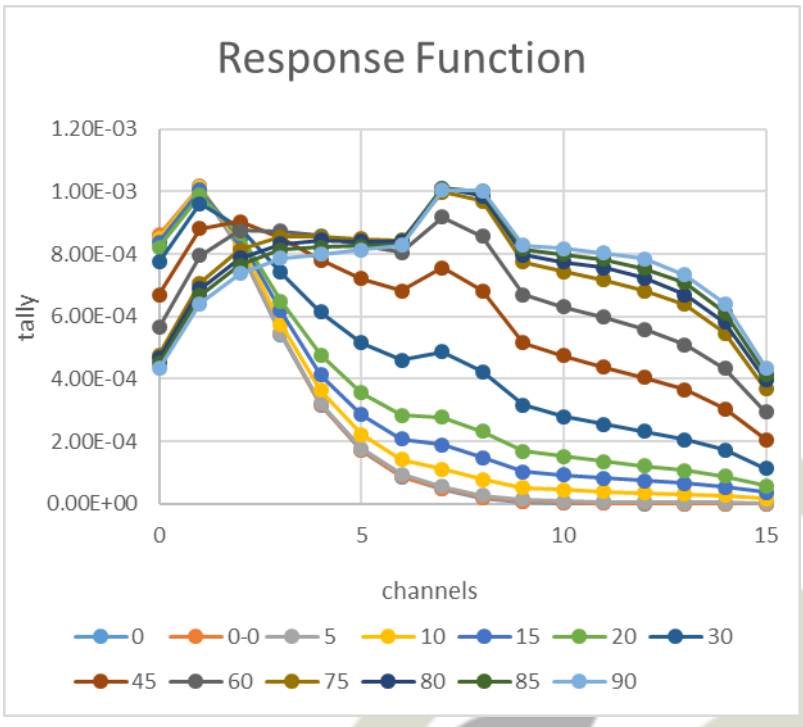

Figure 4-11. Response function vs. incoming angle as determined by MC simulation for two blocks of eight blades

The angles are shown at the bottom of the graph.

Configuration C

Configuration C was more sensitive than configuration B, but the double count rates could not have been determined.

Lessons Learned and Conclusions

The fissile material content of the fuel assemblies could have been demonstrated by neutron count rates under high background condition. Application of shields did not cover the neutron sources. The count rates increased by increasing ^{240}Pu content, but it was not strictly proportional.

The response function gave some information on the type of the shielding.

Configuration B has a directional sensitivity according to MC simulation.

4.2 Neutron Spectroscopic Detectors

4.2.1 European Union (JRC Ispra)

Introduction

The so-called Nested Neutron Spectrometer (NNS) is a Bonner sphere type device based on ^{3}He detector, a set of cylindrical polyethylene moderators of different thicknesses, an electronic chain to measure neutron count-rate vs. moderator thickness and post-processing software (Figure 4-12).

Unaffected by intense gamma-ray fields, the NSS is able to measure:

- Neutron energy spectrum from thermal to 20 MeV (or to GeV with optional addition);
- Neutron fluence;
- Neutron dose-rate;

all of which define its applicability to IPNDV.

Figure 4-12. Principal components of the nested neutron spectrometer (Source: SCK CEN. Used by permission)

In essence, the neutron count-rate versus eight or more HDPE moderator thicknesses are measured. Subsequently one or more unfolding codes are run to characterise the neutrons fields of interest with the knowledge of the detector response functions, and as input the measured count rates and an a priori spectrum. It is worthwhile to note that this a low-energy resolution neutron spectrometer, which might be advantageous in terms of information barrier. However, the determination of neutron fluence is rather accurate.

The main constraints may be mainly time constraints (in non-intense fields) as eight measurements for each moderator thickness need to be performed. For indication, the 61-pin assembly (62% enriched) positioned at 125 cm from the NNS (Figure 4-13), where the neutron fluence was about 40 n/s/cm2, the duration of each measurement was 3-5 minutes and a total measurement time of about 30 minutes, which yielded results with a 2-3% uncertainty.

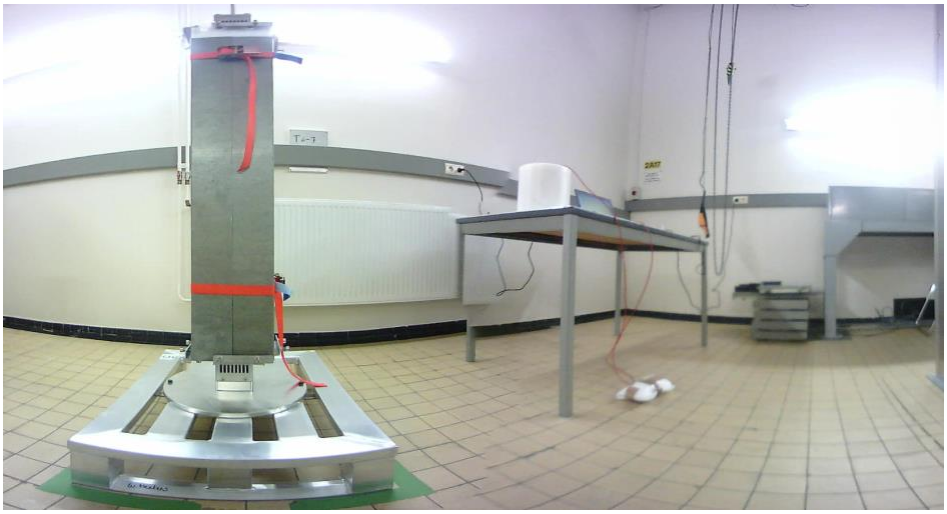

Figure 4-13. 61-pin assembly with HDPE/Cd shield (on the left) and NSS (on the table) at SCK CEN (Be) (Source: SCK CEN. Used by permission)

Specifically, the objects measured with the NSS were the 61-pin (62%) fuel assembly:

- without shield;
- with Cd shield;
- with HDPE + Cd (2 sides) shield;
- with Pb shield.

See Table 4-4 and Figures 4-14 and 4-15.

Results	No Shielding	1.1 mm Cd Shield	50 mm HDPE & 1.1 mm Cd

Expected, n/s	3400000	3400000	3400000
Measured, n/s	7360000	7460000	6000000
Fluence rate, n/s/cm2	37.5	38	30.6
Mean energy (fluence), MeV	1.15	1.18	0.69
Mean energy (dose), MeV	1.94	1.98	1.74
Dose-rate, uSv/h	32.3	33.3 *	17.5

Table 4-4. Selected Measurements Results for 61-pin assembly (62%) with and without shielding

For the cadmium-shielded assembly, the dose rate measured with the Berthold dose rate meter is 20.5 µSv/h compared to 33.5 µSv/h with the NSS, which is reasonably comparable in view of solid angle correction limitations at such small distances and the uncertainties involved with both instruments, especially the Berthold.

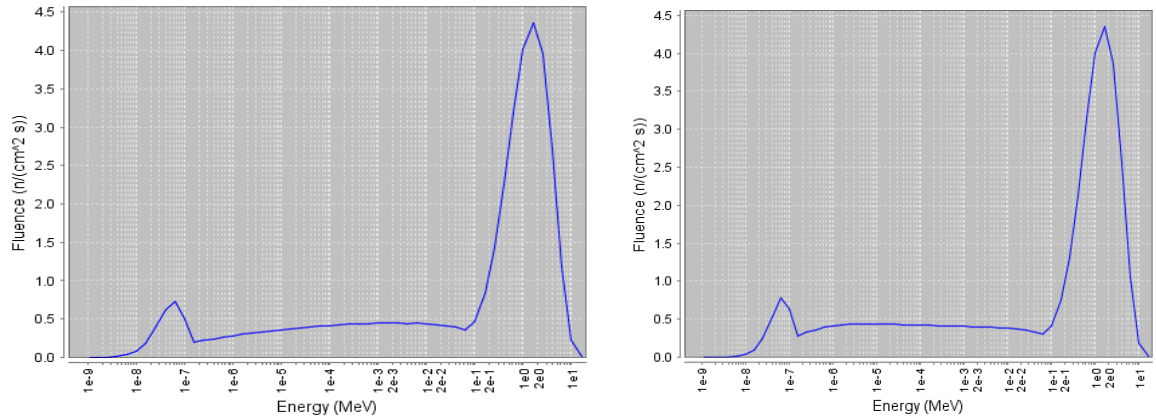

Figure 4-14. Neutron spectrum measured of the 61 pin assembly with and without Cd shield

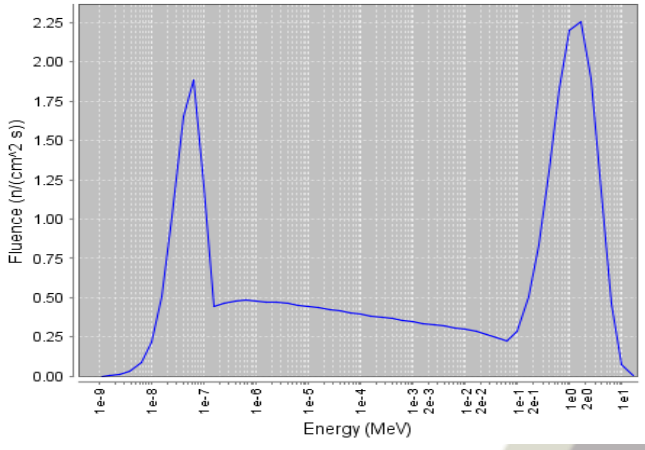

Figure 4-15. Neutron spectrum measured of the 61 pin assembly shielded with HDPE and Cd

Summary and Conclusion

The NSS is capable of measuring with good accuracy be it with low-neutron energy that might be an advantage (IB), the neutron energy spectra, fluence, and dose rates. Mostly due to the high room neutron scattering, the measured neutron flux was generally about twice higher than expected (from calculations). The effect of various shielding on the neutron spectrum, fluence and dose rates were demonstrated. For the cadmium shielded assembly, the dose rate measured with the Berthold dose rate meter is 20.5 µSv/h compared to 33.5 µSv/h with the NSS, which is reasonably comparable in view of solid angle correction limitations at such small distances, the uncertainties involved with both instruments especially the Berthold as well as the high room scatter, which is unaccounted for here. Finally, the low resolution of the neutron spectrometer may help with information barrier requirements and such neutron spectrometry could be adequate for template measurements and absence measurements.

5 Imaging

5.1 Finland (Imperial College, STUK)

Directional and Spectroscopic Neutron Measurements with the nFacet 3D Detector

The nFacet 3D detector is a novel segmented scintillation detector optimized primarily for neutron capture, made up of 64 polyvinyl toluene (PVT) cubes arranged in a 4 × 4 × 4 lattice. Each cube has a ^{6}LiF:ZnS(Ag) screen on three of its six faces, with wavelength shifting fibers set into grooves along each cube. The signal from each fiber is read out by a 3 × 3 mm square SiPM from Hamamatsu. The detector weighs 16 kg and measures 25 × 25 × 27 cm^3, with a photograph of the system visible in Figure 5-1.

Figure 5-1. nFacet 3D detector (Source: SCK CEN. Used by permission)

Although the detector is sensitive to both gamma-rays and neutrons, in this exercise we operated only with a neutron trigger. Incident neutrons thermalize in the PVT, before capturing on the ^{6}LiF:ZnS(Ag) screens. The decay to an alpha particle and a triton causes subsequent excitation and emission of UV scintillation photons in the ZnS(Ag). The scintillation light is collected by two wavelength-shifting fibers (one in each of the X and Y directions) providing spatial localization of the photon signals. The SiPM signal waveforms are collected at the end of the fibre and digitised at 33 MS/s using custom electronics designed for the system.

The segmentation in voxels enables neutron field characterisation and source localization. Measurements of neutron count attenuation in the longitudinal direction provide energy sampling. The vector direction of attenuation, measured through the transverse segmentation, enables source localization. As a result, three-dimensional segmentation provides both full field characterisation and source localization.

Prior to the IPNDV exercise, a series of reference measurements with fission sources were taken at the National Physical Laboratory (NPL) low-scattering neutron facility. The responses

to three common sources were measured: ^{252}Cf, AmBe, and AmLi, giving a good range of mean neutron energies. To demonstrate the level of source discrimination, the neutron rate in planes facing the source across the detector was used to create a profile of stopping power. This is illustrated in Figure 5-2. A simple model based on a decaying exponential was used to fit each source profile to characterize the average attenuation in plane lengths. Even from this simple metric, there is a marked difference in the count rate profile for the different average energy values. This motivates development of a more sophisticated inversion method for source discrimination, which is further explored in the IPNDV exercise.

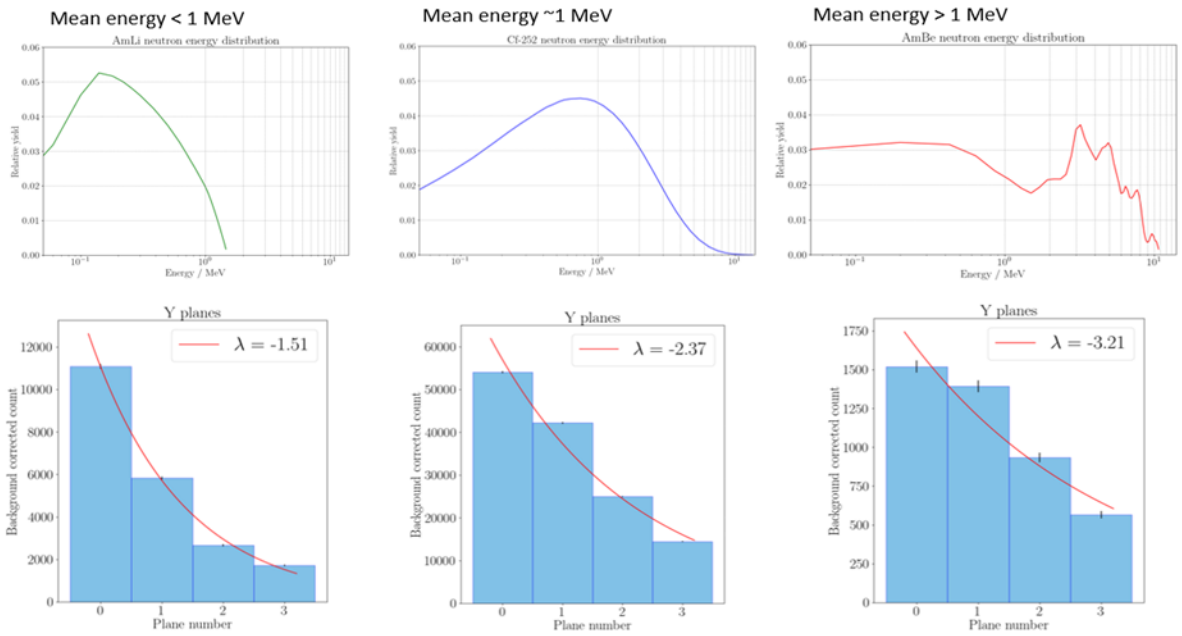

Figure 5-2. Count rate profiles for NPL fission sources

The IPNDV Exercise at SCK CEN

This deployment was the first test of the nFacet system in a real-life scenario with a challenging background. The detector was used to measure MOX fuel assemblies at the Belgian Nuclear Research Centre (SCK CEN), exclusively in neutron mode. Count rate measurements were recorded with and without the MOX assembly present, to characterize both responses to the background and the source separately. The recorded neutron count rates across cubes were used to infer the direction to the source. The rate profile of the MOX assembly was compared with the NPL ^{252}Cf fission measurements. Two detector orientations, at 0° and 90°, were used to assess the angular dependence of the detector response. Measurements of two different assemblies were made, ID 79-16 and ID 96-16, which consisted of 79% ^{239}Pu and a mixture of 96% ^{239}Pu and 79% ^{239}Pu, respectively. These were measured at different distances due to a large difference in neutron activity (at 1.9 m for ID 79-16 and at 0.95 m for ID 96-16). The detector was at a height of 0.91 m from the ground, slightly off axis of the MOX assembly center, which was at a height of 0.37m. Various shielding configurations were studied as a part of the exercise, including Cd and CH_2 + Pb.

Prior to the MOX assembly measurements, neutron background data was recorded. The cube-level data for this survey is shown in Figure 5-3. The background measured consisted of a directional RaBe pile component and a diffuse component from assemblies in adjacent rooms. A background neutron rate of approximately 51 Hz was measured at both distances, resulting in a signal to background ratio of 2:1. This complex background is expressed in the detector, with a large component incident on one edge originating from the pile, identified as thermal neutrons due to a lack of detector penetration. The remaining signal is due to scattered neutrons in the room, which produce small counts incident on other faces.

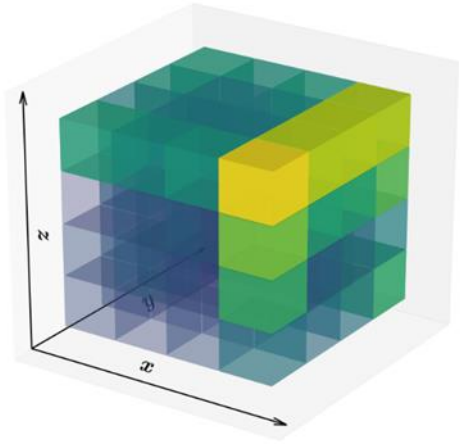

Figure 5-3. Background cube-level counts

Results

Two main results were obtained from the large samples of cube neutron rates collected. First, the direction to the source was reconstructed by fitting a three-dimensional direction vector to the cube rate distribution. Figure 5-4 (a) shows the reconstructed directions, comparing the data after background subtraction. The crosses indicate the true direction to the MOX assemblies in each position. The angular coordinate θ indicates angle in the x-y plane, whereas the radial coordinate φ is the angle made to the x-y plane. The shaded region around each data point indicates the 99.7% (3σ) confidence interval in each direction. The true direction of each source has a φ angle value less than 0° as the detector was at a higher position than the assembly.

At position 1 the θ angle matches the expected value, but in both positions the φ angle is significantly far from the true position of the source. This discrepancy, and the error in the θ angle at position 2, are attributed to two different factors. A first contributing factor to the φ angle is the difference in height between the detector and the source, leading to a larger acceptance for lower cubes than higher ones. In future measurements this effect will be better characterized by testing varying relative heights of source and detector. The second contributing factor is the ^{6}LiF:ZnS screen placement on the detector cube faces; this creates a slight bias in the position of capture, translating into a directional reconstruction bias.

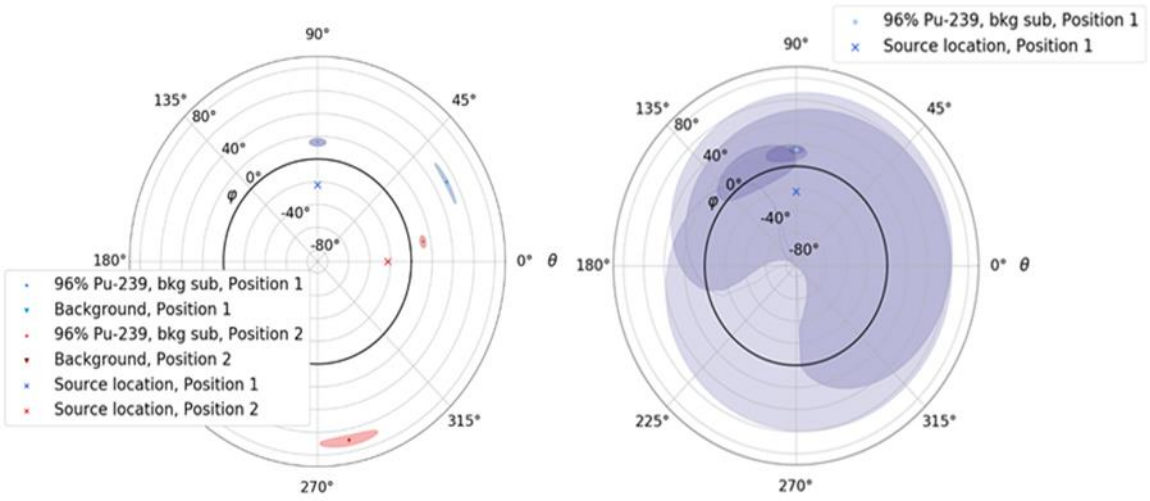

(a) **(b)**

Figure 5-4. (a) direction reconstruction for two positions, with and without the MOX assembly; (b) convergence of uncertainty on direction with increasing neutron count for 10, 100, 1,000, 10,000, and 100,000 neutrons, where the largest region has 10 neutrons and the smallest has 100,000

It is also informative to see how the uncertainty in direction reconstruction converge as the total neutron count increases, as shown in Figure 5-4 (b). Each shaded region indicates the 99.7% confidence region for the reconstructed direction with different amounts of neutrons. The figure shows that after 10,000 neutrons, the reconstructed direction is accurate to within 10°. At typical source rates, the mean direction can be reconstructed at the level of a few degrees in minutes, even with a simple algorithm.

The second result obtained was the source profile analysis, similar to the analysis shown in Figure 5-2. The aim was to see if the measured neutron fluence was consistent with a fission source, such as the ^{252}Cf source measured at NPL. The results of this analysis are shown in Figure 5-5. The bare MOX assemblies are comparable with the characteristic attenuation length in the detector of a fission-like source, but the presence of shielding significantly distorts the view. Although this is only a simple metric, it already gives a good discrimination power between types of neutron sources, suggesting that this detector is capable of precise source discrimination and thus further motivating the development of a more sophisticated inversion method.

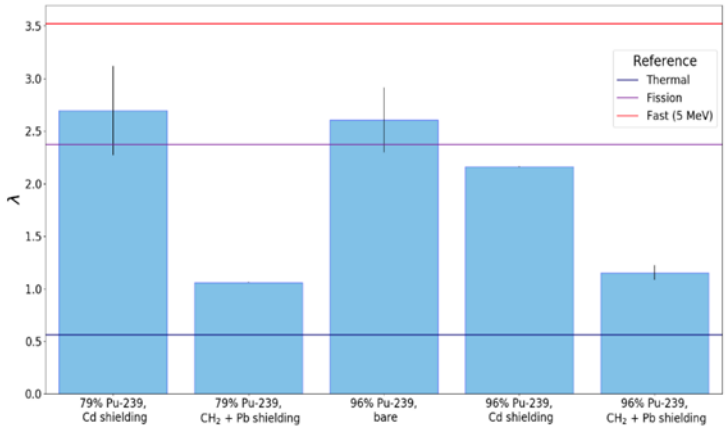

Figure 5-5. Characteristic neutron attenuation lengths in planes for MOX assemblies, compared with reference characteristic lengths

Conclusions

Overall, the IPNDV exercise was a successful test of the nFacet 3D detector in real conditions. A useful dataset of MOX assemblies was collected, and direction reconstruction capabilities were demonstrated. A semi-quantitative measurement of neutron fluence was demonstrated, with development of more sophisticated methods ongoing. Some key areas for improvement were also identified, including compensating for neutron count biases in the detector, an upgrade of the electronics to record both neutrons and gamma-rays and extending measurements to higher neutron source activity.

5.2 Japan (JAEA)

Configurations

- Sample
  - 62 w/o ^{239}Pu: 1 pin, 19 pins, 61 pins
  - 79 w/o ^{239}Pu: 19 pins
  - 62 w/o ^{239}Pu: 19 pins
- Shielding: Bare bundle, Pb: 10 mm; Cd: 2 mm; PE: 50 mm)
- Measurement Distance: 110 cm from center of MOX bundle (Equipment photo
- Figure 5-6)
- Measurement time: 5-10 min

Detector Specifications

- Equipment: Compton gamma imager
- Name: H3D Polaris-H Quad (Equipment photo
- Figure 5-6)
  - Detector: >19 cm^3 CdZnTe
  - Energy resolution: ≦1.1% FWHM @662 keV
  - Radiation FOV: 4π (360°)

- Angular resolution: ~30° FWHM (real time measurement), ~20° FWHM (post process)
- Imaging energy range: 250 keV - 3 MeV
- Sensitivity: localize ^{137}Cs point source with ~3μR/h in <90 sec
- Others: 24 × 9 × 18 cm, 3.5 kg, >6 hr battery life @23°C

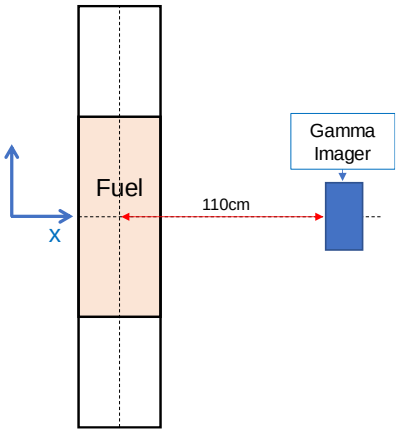

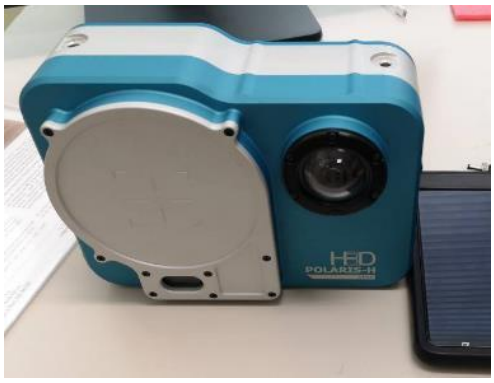

Equipment photo

Figure 5-6. Experimental setup (Source: SCK CEN. Used by permission)

Results and Discussion

The Compton gamma imager can be deployed for presence/absence measurement of plutonium in a countainer and it is possible to be deployed for chain of custody analyses of plutonium by shape change detection of ^{239}Pu (gamma-ray source).

- Imaging of ^{239}Pu source is possible with 5-10 min measurement for about 200 g of WG-Pu (Figure 5-7, Figure 5-8).
- Detailed shape of ^{239}Pu source cannot be recognized, but shape change in 50 cm range can be detected with the measurement at 1 m distance (Figure 5-9).
- Gamma source imaging for <200 keV (i.e., ^{235}U) is not possible with Compton Gamma Imager.

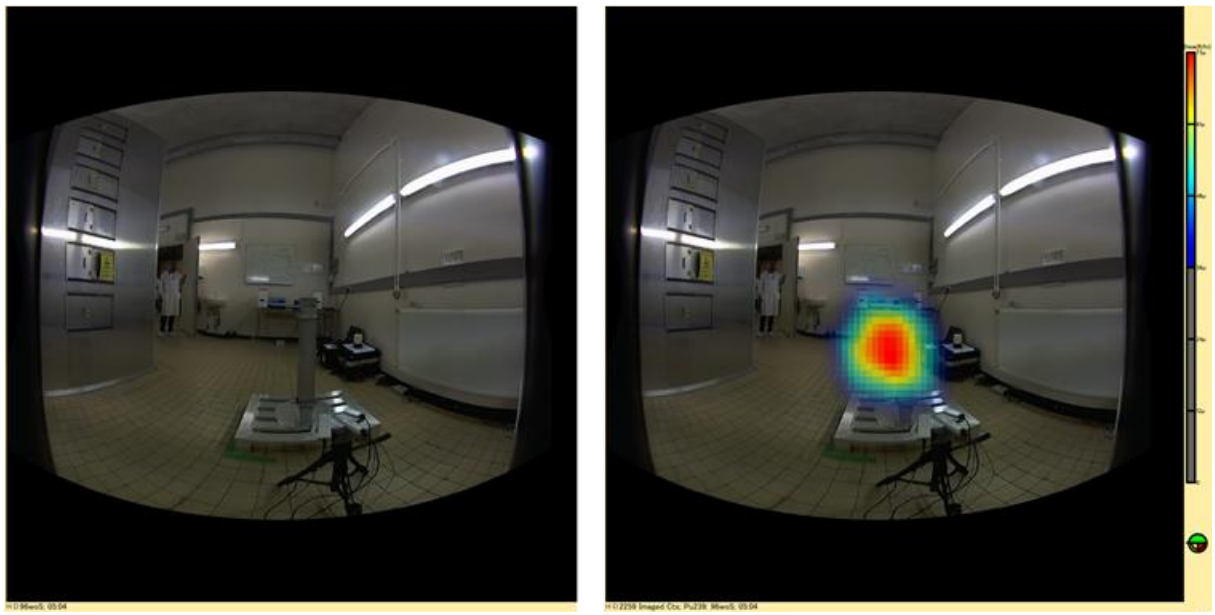

Figure 5-7. Optical image and gamma-ray image of bare MOX bundle (96 w/o ^{239}Pu, 5 min) (Source: SCK CEN. Used by permission)

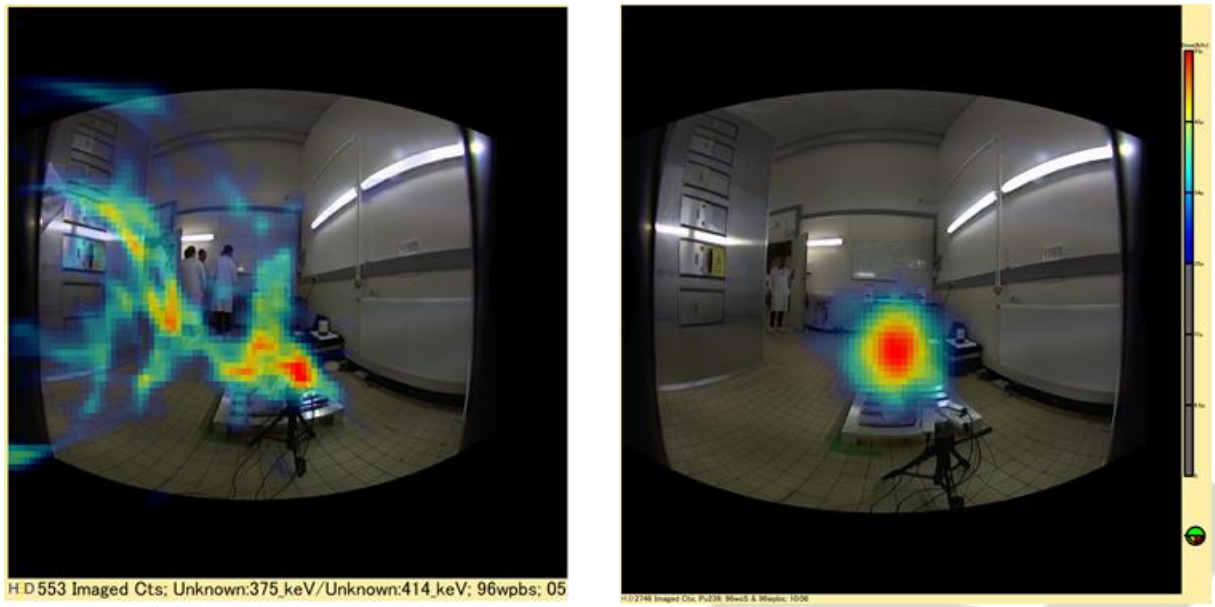

Figure 5-8. Gamma-ray image of MOX bundle with Pb shielding (96 w/o ^{239}Pu, left: 5 min, right: 10 min) (Source: SCK CEN. Used by permission)

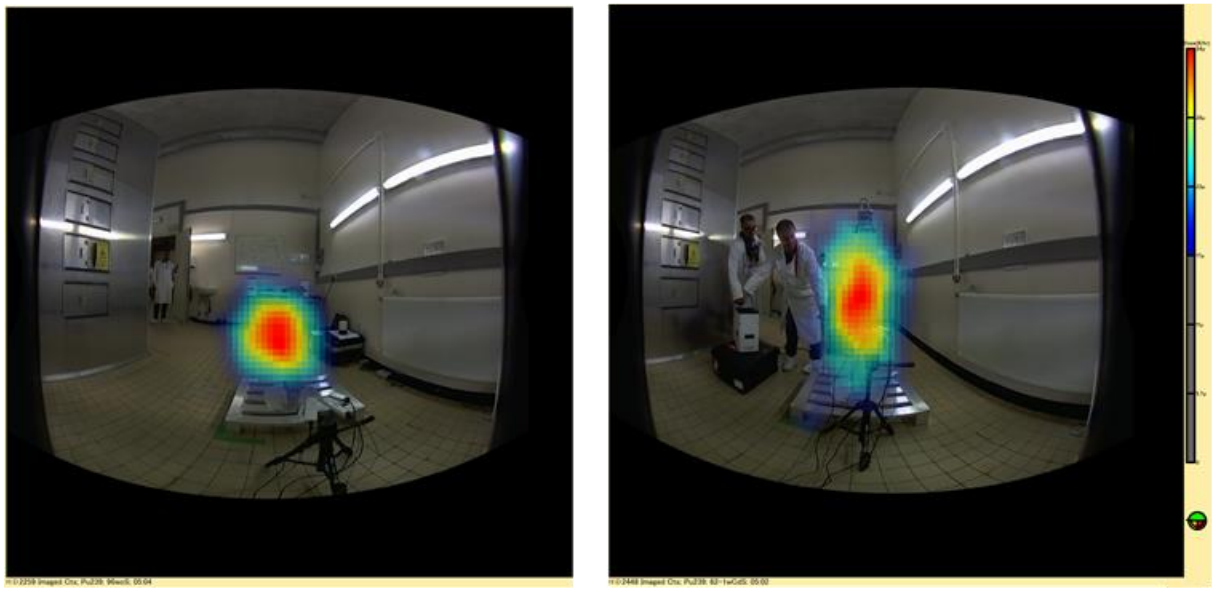

Figure 5-9. Shape change detection by Gamma-ray imaging for bare MOX bundles. 5 min, left: 96 w/o ^{239}Pu (50 cm fuel length), right: 62 w/o ^{239}Pu (100 cm fuel length) (Source: SCK CEN. Used by permission)

5.3 Australia (ANSTO) and EU (JRC-Ispra)

Introduction

This report describes the measurements of a novel gamma-ray imaging system (a prototype CORIS360 imager), designed around the principles of compressed sensing. The described imager can quickly identify and localize gamma emitting radiation over a large field of view (360° × 90°) and across a wide energy range (40 keV to > 3 MeV). The objective of the measurements was to demonstrate the viability of gamma imaging for nuclear disarmament verification. The broad range of MOX fuel pin configurations, provided by the SCK CEN, were imaged and example images will be presented. The interpretation of the measurement results is focused on the imaging capability.

Prototype CORIS360 Specification

The system design consists of a central non-position sensitive CLLBC scintillator detector, surrounded by two nested cylindrical tungsten masks. The CLLBC detector is a dual gamma/neutron scintillator, and for neutron interactions the crystal produces an equivalent gamma energy of 3.1 MeV. The imaging system comes with interchangeable CLLBC detectors in the form of a 0.5” cube and a Ø 1.5” cylinder. For each measurement, the CLLBC detector sees the linear projection of the combined mask pattern on the scene plane. The changing mask pattern effectively encodes the source location information into the detected counts. Gamma images from any part of the measured spectrum can be generated, given there are sufficient counts. The system has four optical cameras that are used to generate a 360^{o} × 90^{o} optical panorama of the scene. The resulting gamma images are overlaid onto this optical panorama, which aids the end user to visualize the location of the gamma emissions. The system is

compact and has an easy-to-use graphical user interface. Key system specifications are given in the table below.

Item	Specification
Spectroscopy Energy Range	40 keV – 3 MeV
Imaging Energy Range	40 keV – 3 MeV
Energy Resolution	~3.5 % @ 662 keV
Detector Type	CLLBC (dual mode: gamma, neutron)
Detector Geometry	Ø1.5” cylinder, 0.5” cube
Optical/Gamma Field of View	360° × 90°
Mask	Tungsten
Max. Angular Resolution	20°
GUI	Real-time image analysis

Table 5-1. Key system specifications for the CORIS360

Results

Figure 5-10 shows the spectral and imaging results for the following MOX fuel pin configuration: 61 pins, 62 %, 1 m long and with 1.1 mm Cd shielding. The spectra and images were those obtained after 3.5 minutes. Figure 5-10 (a) gives the full energy spectrum with the 60 keV ^{241}Am peak ROI between the red lines. This ROI was used to generate the ^{241}Am image in Figure 5-10 (b). Figure 5-10 (b) shows the system generated optical panorama with the overlaid ^{241}Am hotspot location. For this fuel assembly configuration, the cadmium should be shielding the 60 keV ^{241}Am emissions, but the gamma imager has localized emissions coming from a gap in the shielding at the bottom of the assembly. Figure 5-10 (c) shows the same gamma-ray spectrum but with the 375 keV ^{239}Pu peak ROI between the red lines, which was used to generate the gamma image in Figure 5-10 (d). The higher energy gamma emissions (375 keV) can penetrate through the 1.1 mm Cd shielding and the fuel length of the fuel assembly is now showing as a source of radiation. It should also be noted that the spectral peak at approximately 3.1 MeV is due to the neutron emissions from the fuel assembly. The imager was able to identify and localize the ^{241}Am and ^{239}Pu gamma emissions, as well as detect the presence of neutrons.

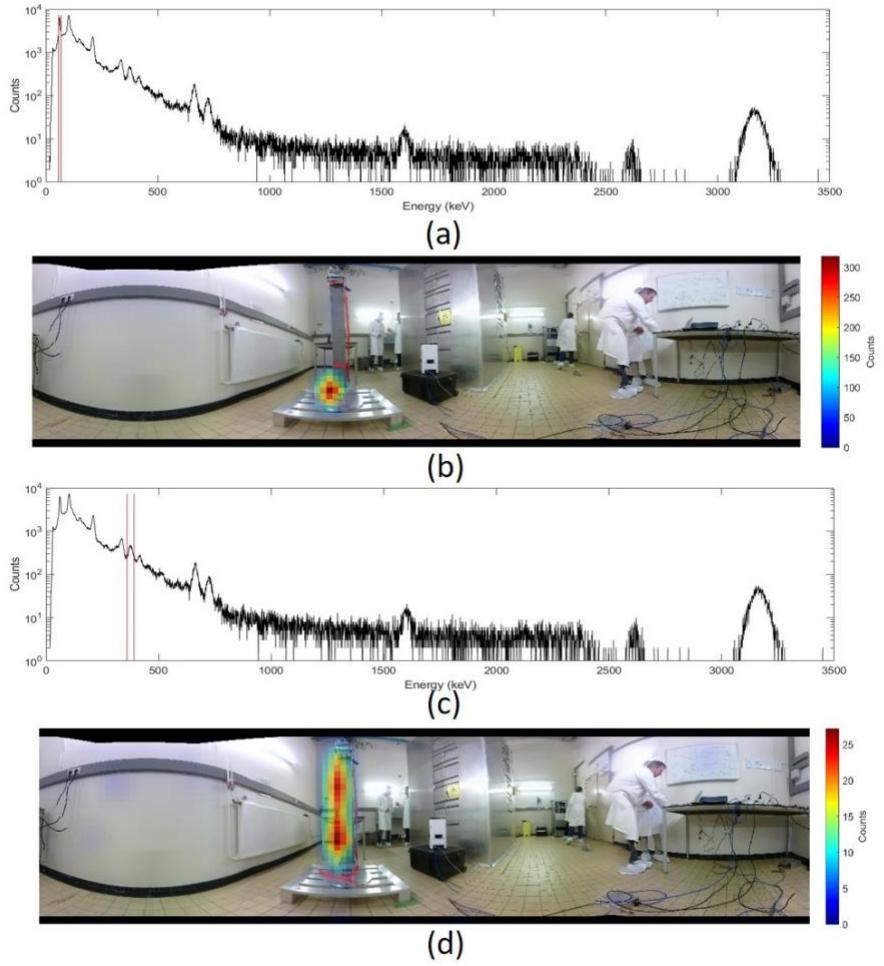

Figure 5-10. (a) The acquired gamma spectrum, from the imaging system, with the 60 keV ^{241}Am peak region of interest (ROI) between the red lines; (b) The resulting ^{241}Am image when reconstructing over the ^{241}Am ROI given in (a); (c) The acquired gamma spectrum with the 375 keV ^{239}Pu peak ROI between the red lines. (Source: SCK CEN. Used by permission)

The results from two prototype CORIS360 imaging systems, setup at 90° to each other, are given in Figure 5-11. Operating two imaging systems in this configuration, and at the same time, can further confine the location information of the detected gamma emissions. Figure 5-11 (a) and (c) show the localization of the 335 keV ^{239}Pu emissions from the two angles. Figure 5-11 (b) and (d) show the localization of the 60 keV ^{241}Am emissions from the two angles. These orthogonal measurements have effectively confined the gamma emissions in three dimensions.

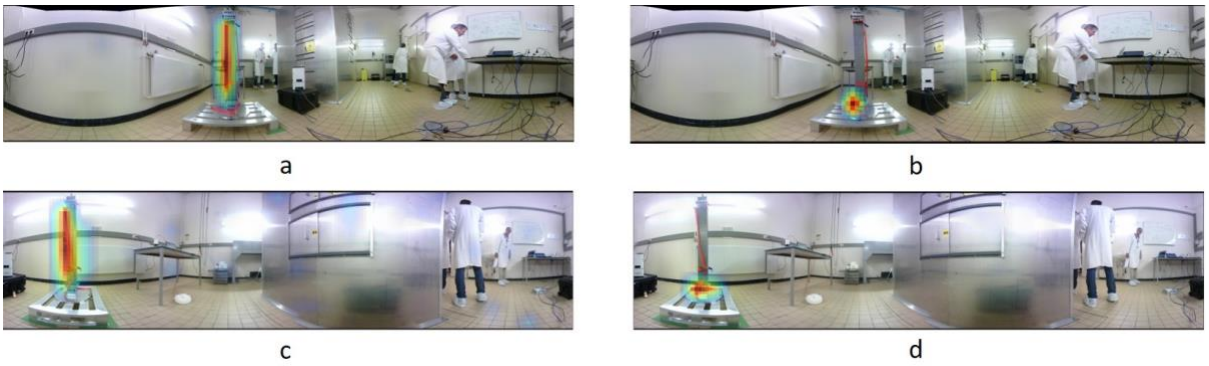

Figure 5-11. Images of the fuel pins taken by two systems arrange at 90° to each other. Images (a) and (c) show the localization of the 335 keV ^{239}Pu emissions; images (b) and (d) show the localization of the 60 keV ^{241}Am emissions. (Source: SCK CEN. Used by permission)

The gamma-ray imaging and spectral results were also obtained for the range of fuel assembly configurations evaluated at the SCK CEN.

Discussion

The gamma imaging technology can be used to identify and localize gamma emissions (i.e., ^{239}Pu and ^{241}Am). The technology can also detect the presence of neutrons. The wide field of view (360° × 90°) enables large areas can be scanned when looking for the absence/presence of nuclear material. The effects of shielding on the fuel pins was clearly evident when the cadmium shielding hid the ^{241}Am emissions from most of the fuel pin length, whereas the higher energy ^{239}Pu emissions could pass through the shielding.

Measurements typically ran for 15-20 minutes, but the imaging technology required just several minutes to localize the gamma emissions. The image and spectral data were available immediately after the measurement had taken place and it only took a few minutes to analyze the data. The elevated neutron background did not create practical problems with the technology.

The results and performance of the gamma imaging technology have confirmed what was written in the Working Group 6 (WG6) technology data sheets. The WG6 spreadsheet states that the storage steps are appropriate due to the longer measurement times. However, the demonstrated shorter measurement times might mean that gamma imaging could be used in more steps. When considering the requirement of an IB, the broad shape of the plutonium gamma emissions could be seen, but not in high-resolution detail. There would be a need an information barrier for high-resolution images. However, it should be noted that the image resolution can be tailored through the system design.

The system setup is straight forward and only takes a few minutes. The imager requires a laptop to operate and power to run. An energy calibration maybe required after the transportation of the device. The technology takes optical photos, which may be problematic when operating in classified areas.

The measurement campaign demonstrated that gamma-ray imaging could be used for nuclear verification purposes. The gamma imager was able to identify and localize the gamma emissions from the fuel pins, as well as detect the presence of neutrons. If the measurement campaign were to be repeated, then it would be interesting to perform measurements at closer positions. The CORIS360 gamma imaging technology is also looking to expand the imaging capability to include thermal neutrons. Therefore, there would be considerable interest in evaluating the polyethylene shielded scenarios with both the gamma and thermal neutron imaging capabilities, in the future.

6 Implications for Nuclear Disarmament Verification

The Belgian measurement campaign much benefited from the substantial number of analytical techniques used by the various teams. These covered most of the passive radiation measurement technologies identified by the IPNDV Technology Working Group as potentially applicable for nuclear disarmament verification.

As documented in detail in this report, the information given in the IPNDV Technology Data Sheets on potentials and limitations of the measurement technologies applied in the measurement campaign have been confirmed.

However, the campaign showed various additional results with potential implications on the choice of nuclear disintegration measurement techniques for disarmament verification. These are summarized in the following.

High-Resolution Gamma Detection

As expected, this technique allows determining the ^{240}Pu:^{239}Pu isotopic ratio as a generally accepted attribute and thus verifying the presence of weapons grade plutonium. In addition, the measurement campaign documented that it also works in case of high-gamma background.

The technology is sensitive to shielding by high Z material (e.g., iron, lead), which effectively shields gamma signals below about 300 keV. However, the presence of such shielding becomes apparent from its x-ray lines. Plutonium gamma lines with energies above 600 keV are much less sensitive to shielding, but count rates are lower and may require long data acquisition times.

Due to its sensitivity to shielding, the applicability of gamma detection for attribute verification may be limited by the potential presence of a reflector or tamper, but is attractive after disassembly (step 8 of the IPNDV disarmament process scheme).

Medium-Resolution Gamma Detection

Of the various detector materials tested, CdZnTe and $LaBr_3$ as well as NaI showed energy resolutions that allowed interpreting the spectra, but GAGG and CsI detectors did not. For CdZnTe and $LaBr_3$ considerable research and development achievements are required—in particular, manufacturing larger crystals and developing peak evaluation procedures.

Determination of the plutonium isotope ratio as attribute was not successful.

As documented for the NaI and CdZnTe detector, medium resolution detectors are attractive for gamma template measurements.

Neutron Counting

Both ^{3}He and scintillation detectors are available, which detect plutonium masses down to approximately 500 g with hand held devices.

For absence measurements of plutonium, high-volume ^{3}He detectors and arrays of scintillation detectors can be used.

Neutron scattering by walls and floor may obscure the emitted signal and thus any directional analysis.

Neutron counting is attractive for verifying the presence or absence of plutonium at any position of the IPNDV dismantlement process scheme.

Nested neutron spectrometers and arrays of scintillation detectors may provide spectral information, which allow verifying the presence of a source of fissile material and of moderating material, but could be applied for template measurements also. However, neutron reflection on building structures may invalidate spectral analyses of the unscattered source neutrons.

Neutron Coincidence Measurements

The technology is applicable even with high background of uncorrelated neutrons as caused by (α,n) reactions of the oxide.

Masses of ^{240}Pu and—if the isotopic ^{239}Pu:^{240}Pu ratio is known—of total plutonium are well estimated for unmoderated configuration down to 20 g. At such low masses an accurate background correction is important and the technology showed to be sensitive to the presence of high-density polyethylene shielding.

Gamma/Neutron Imaging

Imaging technologies are available that allow both the localization of gamma- and neutron-emitting sources, respectively. Two images from different perspectives are required for a three-dimensional determination of a source's position.

Images reflect the sources' shape, but show limited spatial resolution.

Both gamma and neutron imaging technologies are applicable for verifying the presence as well as the absence of plutonium, but not for attribute analyses (plutonium isotopic ratio).

Ideally, an imaging device including gamma and neutron detectors could be applied, because intentionally masking any passive radiation signal would require quite sophisticated shielding, which could be detected by other verification activities (e.g., by noting modifications of the room structure or by checking empty containers). Such an imaging device could be applied at any position of the IPNDV dismantlement process scheme.

7 Conclusions and Outlook

The measurement campaign became a major contribution to the overarching goal *"From Paper to Practice"* of Phase II of the International Partnership for Nuclear Disarmament Verification thanks to various plutonium configurations provided by the Belgian organizers and to the engagement of the many teams performing measurements with differing technologies.

The campaign confirmed that the information given in the Technology Data Sheets developed during Phase I of IPNDV is adequate, but also documented that emerging gamma and neutron detector materials show high potentials for being applied for verification measurements.

The Belgian measurement campaign also provided an almost unique data base for validating neutron and gamma simulation codes for applying these in nuclear disarmament analyses.

Based on the experience gained and documented by this report various suggestions for future measurement campaigns have been made. These include:

- All teams expressed a high interest in a measurement campaign as "blind test," i.e., without any prior information on the configurations analyzed (material, isotopic composition, geometry, shielding, etc.).
- The performance of the various gamma detection technologies for highly enriched uranium with limited external shielding should be assessed.
- The sensitivity of the gamma and neutron imaging technologies to shielding should be studied systematically.
- For spectrometric neutron technologies blind tests should include discriminating between plutonium and neutron sources (e.g., ^{252}Cf) as well as between plutonium in oxide and metal form.

Acknowledgments

This is a product of the IPNDV Working Group 6: Technologies for Verification and the Technology Track, organized and compiled by:

Alessandro Borella, Belgium delegate to IPNDV, Senior Researcher, Nuclear Science and Technology Studies Unit, SCK CEN

Gerald Kirchner, German delegate to IPNDV, Head of the Carl-Friedrich von Weizsäcker Centre for Science and Peace Research of the University of Hamburg

Participants' List

Team/Delegation	Participants	Affiliation
Australia	David Boardman	ANSTO Sydney
Australia	Alison Flynn	ANSTO Sydney
Belgium	Alessandro Borella	SCK CEN Belgian Nuclear Research Centre
Belgium	Riccardo Rossa	SCK CEN Belgian Nuclear Research Centre
Belgium	Klaas van der Meer	SCK CEN Belgian Nuclear Research Centre
Canada	Ghaouti Bentoumi	Canadian Nuclear Laboratories (CNL)
Canada	Liqian Li	Canadian Nuclear Laboratories (CNL)
European Union	Francesco Raiola	Joint Research Centre Ispra
European Union	Arturs Rozite	Joint Research Centre Ispra
European Union	Hamid Tagziria	Joint Research Centre Ispra
Finland	Anders Per Axelsson	FOI (Swedish Defence Research Agency)
Finland	Antonin Vacheret	Imperial College London
Finland	Kari Peräjärvi	STUK (Radiation and Nuclear Safety Authority)
Germany	Manuel Kreutle	Universität Hamburg
Hungary	István Almási	Hungarian Academy of Sciences (MTA)
Hungary	Zoltán Hlavathy	Hungarian Academy of Sciences (MTA)
Hungary	Gergely Dósa	Hungarian Academy of Sciences (MTA)
Japan	Satoshi Suzuki	E&E Techno Service Co., Ltd
Japan	Yoshiki Kimura	Japan Atomic Energy Agency (JAEA)
Norway	Kjell Olav Johansson	IFE Kjeller
Norway	Tore Ramsøy	IFE Kjeller
Norway	Naeem Ul Hasan Syed	DSA (Norwegian Radiation and Nuclear Safety Authority).
NTI	Andrew Newman	Nuclear Threat Initiative (NTI)
Switzerland	Rolf Althaus	Spiez Laboratory
Switzerland	Christoph Wirz	Spiez Laboratory
United Kingdom	Jake Deeming	Atomic Weapons Establishment (AWE)
United Kingdom	Paul Richard Knight	Atomic Weapons Establishment (AWE)
United Kingdom	Jennifer Schofield	Atomic Weapons Establishment (AWE)
United Kingdom	Joshua Henry Smith	Atomic Weapons Establishment (AWE)

About the IPNDV

For more information on the IPNDV Working Groups, please see www.ipndv.org/working-groups.

The IPNDV is an ongoing initiative that includes more than 25 countries with and without nuclear weapons. Together, the Partners are identifying challenges associated with nuclear disarmament verification and developing potential procedures and technologies to address those challenges.

The IPNDV is working to identify critical gaps and technical challenges associated with monitoring and verifying nuclear disarmament. To do this, the Partnership assesses monitoring and verification issues across the nuclear weapon lifecycle.

The IPNDV is also building and diversifying international capacity and expertise on nuclear disarmament monitoring and verification. Through the Partnership, more countries understand the process, as well as the significant technical and procedural challenges that must be overcome. At the same time, the Partnership is highlighting the importance of verification in future reductions of nuclear weapons.